Journal of
Materials Chemistry B

Materials for biology and medicine

Accepted Manuscript

This article can be cited before page numbers have been issued, to do this please use: D. D. Sall, Y. Xiao, A. K. D. Diaw and M. Hémadi, *J. Mater. Chem. B*, 2026, DOI: 10.1039/D6TB00190D.

This is an Accepted Manuscript, which has been through the Royal Society of Chemistry peer review process and has been accepted for publication.

Accepted Manuscripts are published online shortly after acceptance, before technical editing, formatting and proof reading. Using this free service, authors can make their results available to the community, in citable form, before we publish the edited article. We will replace this Accepted Manuscript with the edited and formatted Advance Article as soon as it is available.

You can find more information about Accepted Manuscripts in the Information for Authors.

Please note that technical editing may introduce minor changes to the text and/or graphics, which may alter content. The journal's standard Terms & Conditions and the Ethical guidelines still apply. In no event shall the Royal Society of Chemistry be held responsible for any errors or omissions in this Accepted Manuscript or any consequences arising from the use of any information it contains.

ROYAL SOCIETY OF CHEMISTRY

rsc.li/materials-b

View Article Online
DOI: 10.1039/D6TB00190D

ARTICLE

Application of Carbon Dots and Their Composites to Analysis of Heavy Metals and Small Biomolecules by Fluorescence Spectroscopy

Received 00th January 20xx,
Accepted 00th January 20xx

DOI: 10.1039/x0xx00000x

Diébel Dado Sall[#a,b], Yawen Xiao[#a], Abdou Karim Diagne Diaw[b] and Miryana Hémadi*[a]

Carbon Dots (CDs) have attracted significant attention due to their unique photoluminescent properties, biocompatibility, and versatile surface functionalities. After a brief introduction devoted to their synthesis and characterization, this review explores the fluorescence properties of CDs, and how these are impacted by non-metallic and metallic atom doping, surface functionalization and passivation. Applications of CDs for analyzing heavy metals and small molecules of biomedical interest by fluorescence spectroscopy are discussed. CD composites with inorganic or organic materials are presented along with applications to both the assay and removal of heavy metal and organic pollutants. Challenges and future prospects in this emerging field are addressed.

1. Introduction

Water pollution is a very serious problem that has been exacerbated by the process of industrialization, the expansion of urban areas, and agricultural practices. Water sources have become extensively polluted with a multitude of detrimental substances, notably heavy metals like lead, mercury, and cadmium, as well as a variety of organic pollutants such as pesticides and pharmaceuticals [1,2] . The distribution of these pollutants is closely associated with human population densities, particularly in heavily industrialized areas of Europe, North America, and Oceania, leading to a profound ecological and public health crisis [3]. The adverse effects range from the degradation of aquatic ecosystems to the emergence of chronic health conditions in humans, emphasizing the urgency for innovative and effective treatments.

Given the complexity of water pollution, characterized by a vast array of chemical contaminants, the development of highly sensitive and selective detection methods is imperative [4]. Traditional approaches often fall short, unable to adequately address these concerns due to limitations in sensitivity, specificity, and operational feasibility. Therefore, the ability to detect and accurately quantify pollutants, particularly at low concentrations within complex environmental matrices, is critical for the monitoring and treatment of water pollution.

Within this context, Carbon Dots (CDs), a novel class of nanomaterials, have shown immense promise as a means of improving the analysis of heavy metal ions [5,6]. Their size, less than 10 nm, their notable fluorescence, and customizable surface functionality permit the design of specialized sensors that are highly sensitive and selective. Offering advantages over traditional detection methodologies, including reduced toxicity, environmental compatibility, and the capacity for real-time monitoring, CDs stand out as a formidable tool in environmental science. Reflecting the increasing relevance of CDs, data collected and visualized in recent publications reveal an escalating trend in research, particularly in

[a] Université Paris Cité, ITODYS, CNRS-UMR 7086, F-75013 Paris, France.
[b] Laboratory of Organic Physical Chemistry and Environmental Analyses (LCPOAE), Department of Chemistry, Faculty of Sciences and Techniques, Cheikh Anta Diop University, PO-BOX 5005, Dakar-Fann, Senegal.
[#] Contributed equally to this work
*Corresponding author

View Article Online
DOI: 10.1039/D6TB00190D

sensor applications, which have surged to comprise 47% of all CD-related research by July 2025. This surge responds to the important demand for advanced sensing technology in water pollution control.

This review paper concentrates on the versatile applications of these nanomaterials in addressing the challenges of heavy metal quantification (essentially by CDs) and remediation (essentially by CD composites) in aqueous systems. However, the possibilities for exploiting the fluorescence properties of CDs are not limited to heavy metals. They can also be applied to the detection and quantification of small molecules of biomedical interest by fluorescence spectroscopy. It seems appropriate therefore to combine these two aspects in a single review,
despite the difference in their fields of application.

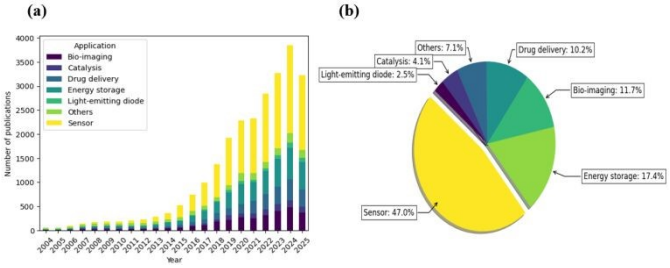

Figure 1. Publication trends of CDs (2004-2025) (a) Annual distribution across various application areas, (b) Proportional breakdown by field, data sourced from Scopus as of July 2025.

2. Synthesis of Carbon Dots

CDs offer a versatile platform for environmental monitoring, their synthesis and modification dictating their physicochemical properties. CD preparation methods are classified according to the raw materials used for their preparation, and can be divided into top-down and bottom-up routes. The "top-down" approach consists in breaking down carbonaceous materials to form nano-sized CDs by physical or chemical methods, including laser ablation and electrochemical exfoliation. The precursors are mainly: graphite powder [7], graphene/graphite oxide [8,9], activated carbon [10,11], carbon nanotubes [12], and candle soot [13]. Conversely, the "bottom-up" approach consists in taking a carbon-containing organic material as the precursor, and preparing CDs by carbonization, pyrolysis, microwave-assisted synthesis, and hydrothermal/solvothermal methods. Commonly used materials include: small organic molecules (acetic acid [14], sugars [15], amino acids [16], citric acid [17], urea [18], folic acid [19]), polymers (proteins [20], linear polymers [21], polythiophene [22], chitosan [23], DNA [24]), biomass materials (papaya leaves [25], bamboo leaves [26], fruits [27], flower petals [28]), and mixtures of several source materials. The surface of CDs allows for a plethora of modification techniques including, but not limited to, functionalization with organic or inorganic molecules, doping with heteroatoms like nitrogen or phosphorus, and coating with biocompatible materials. These alterations can enhance solubility, specificity, and the overall detection capability of CDs, paving the way for their use in diverse environments.

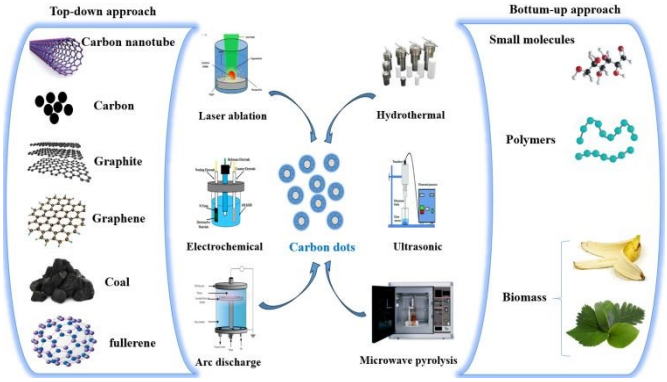

Figure 2. Two approaches to obtaining CDs (bottom-up and top-down)

2.1 Top-down approach

2.1.1 Electrochemical/chemical oxidation

Electrochemical/chemical oxidation is the predominant top-down synthesis method for producing CDs. This approach offers several notable advantages, including high yield, high purity, low cost, and easy size control [29]. The choice of electrolyte and electrode materials is important insofar as it makes it possible to generate CDs with distinctive fluorescence emission, cytotoxicity, and surface state characteristics. Various conductive carbon materials (carbon fiber, graphite rod, etc.) serve as sacrificial electrodes [30,31].

Rocco et al. [32] demonstrated that the selection of the electrolyte significantly influences the optical properties of electrochemically synthesized CDs. Using graphite rods as sacrificial electrodes in a $K_2S_2O_8$ electrolyte resulted in red-emissive CDs, attributed to sulfate radical-mediated exfoliation. In contrast, the use of PBS or a citric acid/NaOH electrolyte yielded blue-emissive CDs with oxygen-rich surface functional groups. In related studies, graphene quantum dots (GQDs) and graphene oxide quantum dots (GOQDs) were prepared by electrochemical exfoliation of graphite rods in a two-electrode cell configuration (Figure 3a) [33]. A practical one-step strategy for the synthesis of GQDs, based on the electrochemical stripping of a coke

View Article Online
DOI: 10.1039/D6TB00190D

working electrode, has been developed (Figure 3b) [34]. By regulating the current density applied to the coke and the water content of the electrolyte solution, the emission wavelengths of the GQDs can be precisely controlled, resulting in green (G-GQDs), yellow (Y-GQDs) and orange (O-GQDs) fluorescent materials with yields of 18, 43 and 31 wt.%, respectively. In addition, the G-GQDs prepared can be reduced by $NaBH_4$ to form new GQDs with blue fluorescence (B-GQDs) (13 wt.% yield).

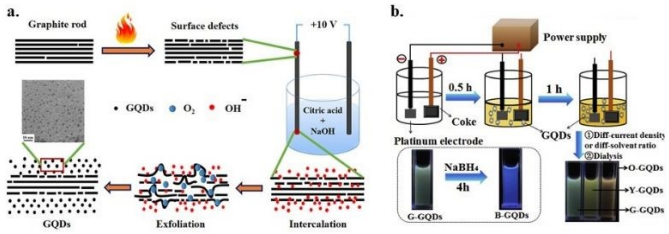

Figure 3. (a) Electrochemical exfoliation of defect-induced graphite rod. Intercalation of OH^- ions, O_2 production, and exfoliation result in GQDs. Reproduced from ref. 33 with permission from the American Chemical Society, copyright© 2017. (b) Synthesis of multicolor GQDs from coke. Reproduced from ref. 34 with permission from Elsevier Ltd, copyright© 2018.

2.1.2 Laser ablation

In laser ablation a carbon source is subjected to laser irradiation which produces very high plasma temperatures and pressures at the solid-liquid interface. Explosive sputtering melts the surface of the target, resulting in the formation of nanodroplets. A low-pressure vapor medium is preferable as it favors the generation of smaller nanoparticles with little chance of aggregating [35]. The properties of the CDs depend on the nature of the target and the medium, as well as the properties of the laser used (wavelength, power density, pulse duration, etc.), making this process versatile in terms of customized CD production [36]. Recent work by Cortes et al. [37] further highlights the versatility of pulsed laser ablation in liquids (PLAL) for synthesizing high-purity carbon and graphene quantum dots, emphasizing the influence of laser parameters and solvent type on size, composition, and photoluminescence properties.

Single-step pulsed laser ablation (PLA) of graphite was used to fabricate amine-functionalized GQDs (FGQDs) using polypyrrole as both precursor (N-amine) and surfactant (Figure 4) [38]. Due to the synergistic effect of surface passivation and the incorporation of N-amine groups, FGQDs showed a sensitive response to Fe^{3+} ions with a limit of detection (LOD) of 500 nM.

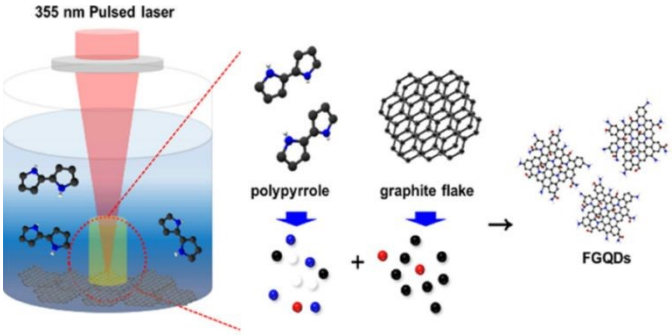

Figure 4. Possible mechanism for the transformation of graphite flakes to FGQDs by PLA. Reproduced from ref. 38 with permission from the American Chemical Society, copyright© 2022.

2.1.3 Ultrasonic treatment

Large carbonaceous materials can be broken down by the mechanical energy of ultrasonic sound waves (>20 kHz). This treatment combines mild processing conditions with enhanced product yield [35], and offers several advantages, including simplicity, affordability and scalability, as well as precise control over the size, shape, and surface characteristics of the resulting CDs [39,40].

The properties of the resulting CDs can be tailored by adjusting parameters such as ultrasonic power, reaction time, solvent type, and carbon precursor ratios. For instance, Huang et al. [41] used a direct ultrasonic exfoliation method to synthesize chlorine-doped graphene quantum dots (GQDs). Similarly, Park et al. [42] used ultrasonic treatment on a mixture of ethanol and food waste to prepare water-soluble carbon quantum dots (CQDs). This process yielded CQDs (average particle size 2–4 nm) having strong photoluminescence, good photostability, and low cytotoxicity, making them highly promising for in vitro bioimaging applications.

2.2. Bottom-up approach

2.2.1 Hydro/solvothermal synthesis

Hydrothermal and solvothermal methods are among the most widely employed bottom-up strategies for synthesizing carbon dots (CDs), due to their simplicity, low cost, environmental friendliness, and the possibility of tailoring their physicochemical properties. In both approaches, organic precursors such as saccharides, amines, organic acids, or their derivatives are subjected to thermal treatment in a sealed high-pressure reactor (typically PTFE-lined), allowing

carbonization, dehydration, polymerization and cross-linking to proceed under controlled temperature and pressure conditions [43–45]. These reactions are typically conducted at temperatures ranging from 120 to 260 °C for several hours, using either water (hydrothermal) or organic solvents (solvothermal) as the reaction medium. By a combination of precursor design, thermal control, and solvent selection, CDs with varied emission colors, surface functionalities, morphologies, and dopant profiles (e.g., N, S, Fe, or Se) can be obtained. This flexibility is key for tailoring CDs to specific applications.

The hydrothermal method is used by most researchers as an inexpensive, and sustainable route for CD synthesis [43–45]. In this method the reaction mixture in water is held in an autoclave at 120–240 °C for several hours under the autogenous pressure of the solution within the sealed system. For instance, fluorescent 1.72 nm-diameter CDs were synthesized by heating solutions of ammonium citrate and ammonium thiocyanate at 160 °C for 6 h [46]. Similarly, L- or D-cysteine-derived CDs were obtained via a one-step hydrothermal treatment at 150 °C for up to 20 h [47]. Iron- and nitrogen-doped CDs (diameter 3.7 nm) were prepared by heating ferric chloride and Na_2EDTA at 200 °C for 10 h [48]. CDs doped with N and S (diameter 5–7 nm) for Fe^{3+} detection (LOD, 0.2 μM) were synthesized hydrothermally from citric acid and thiourea by heating at 180 °C for 12 h [49].

Under solvothermal conditions, p-phenylenediamine was used to obtain 3.6 nm CDs in ethanol or dimethylformamide (200 °C, 6 h) [50], while N-doped CDs (NCDs) were prepared at 260 °C from PET oligomers, pyromellitic anhydride and urea in tetrahydrofuran [51]. In another example blue-emitting CDs (2.8–3.2 nm) were synthesized by heating folic acid in formamide at 160 °C [52].

2.2.2 Microwave-assisted Synthesis

Microwave-assisted synthesis is a fast, clean, sustainable, and cost-effective method aligned with Green Chemistry. Its primary advantage is that energy is generated directly within the material through molecular interactions [53,54] with the electromagnetic field [55,56], allowing efficient and uniform heating. This results in reduced thermal inertia [57] and significantly shorter reaction times than for conventional methods [58,59] (Figures 5a,b). Additionally, it improves safety, reproducibility, and precise experimental control while optimizing particle size and ensuring a high-yield production of size-controlled CDs [60].

Heteroatom-co-doped CDs were synthesized by microwave heating at 500 W for 20 min. [61]. and SD-CDs were synthesized from 5-sulfo-anthranilic acid and 1,5-diphenylcarbazide by this method (600 W, 10 min.)[62]. Highly fluorescent nitrogen-sulfur co-doped CDs (NS-CQDs) were prepared from L-cysteine and citric acid (800 W, 60 s) [63].

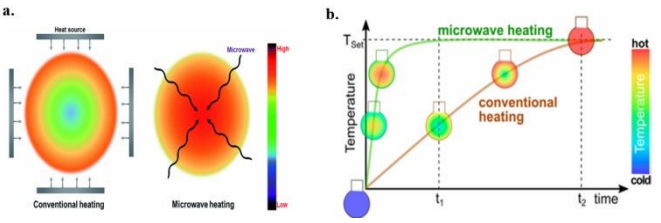

Figure 5. (a) Schematic presentation of the initial spatial temperature profiles in a spherical reactant solution during conventional heating (left) and microwave-assisted heating (right). Reproduced from ref. 58 with permission from Springer nature B.V., copyright© 2018. (b) Different temperature transients that result from conventional heating and microwave-assisted heating. Reproduced from ref. 59 with permission from Sage publications, copyright© 2018.

2.2.3 Pyrolysis methods

The pyrolysis method involves heating precursors at very high temperatures under controlled conditions to induce a series of dehydration, polymerization, and carbonization reactions [64]. Temperature is a critical parameter: insufficient heat can lead to incomplete carbonization, whereas excessive temperatures may cause over-oxidation, damaging the surface of CDs and impairing their optical properties. Similarly, the reaction time must be optimized to avoid under- or over-carbonization [65].

In some protocols, especially when dealing with complex or polymeric carbon precursors, strong acids or bases may be employed prior to or during pyrolysis to facilitate the decomposition and enhance carbonization efficiency [66,67]. These chemical agents can also promote the removal of heteroatoms or introduce functional groups, which can significantly impact the physicochemical and optical properties of the resulting CDs. Thus, even within thermal processes like pyrolysis, the chemical environment, including the pH, can play a supporting role in tuning CD formation. Due to its many advantages (simple operation, short reaction time, wide precursor tolerance and low cost), this method has frequently been used in recent years for research into the large-scale preparation of CDs [68,69].

View Article Online
DOI: 10.1039/D6TB00190D

Graphene quantum dots (GQDs) and nitrogen-doped graphene quantum dots (N-GQDs, for Cu^{2+} ion detection) were prepared by direct pyrolysis of citric acid and urea (200 °C, 30 min.) [70]. Using a one-step pyrolysis approach, citric acid (CA) and ethylenediamine (EDA) were thermally treated to synthesize N-doped carbon dots (NCDs) with a high mass yield of 69% and a quantum yield of 65.5%, without post-treatment. The resulting NCDs exhibited excitation-independent blue fluorescence and were successfully applied for the selective detection of Fe^{3+} in buffer solution, with a low detection limit (0.703 µM) and good performance in real water samples [71].

3. Purification and separation of CDs

Beyond the previously mentioned techniques, several other notable approaches can be employed for the synthesis of CDs, including self-assembly, anchor/support-based strategies, and metal-organic framework (MOF) template methods. Uniformity and precise size control are essential for their applications and can be further optimized by post-treatment processes. The removal of impurities, such as unreacted compounds and by-products, plays a critical role in ensuring the quality and compatibility of CDs. Although no universal method exists for their purification and separation, specific protocols can be developed according to the nature of the products obtained after the synthesis process. Many techniques, including dialysis, filtration, centrifugation, precipitation, and column chromatography, capillary electrophoresis, ion-exchange, have been explored in the literature, each offering distinct advantages in addressing impurity-related challenges [72–76]. Various methods applied to isolate CDs from other reaction materials (starting products, oligomers, aggregates, microparticles) are reported in Figure 6. The required purity level may vary depending on the application. Due to the diversity of CD structures and synthetic pathways, purification procedures must be adapted accordingly. As a result, many studies opt to use or characterize CDs directly within composite systems, where purification is less critical, rather than isolating them in their pure form [77].

Filtration involves forcing the crude CD reaction mixture through a filter or membrane to separate and remove the larger particles. For effective purification, PTFE filters with pore sizes ranging from 0.22 µm to 0.45 µm are commonly used. Dialysis follows, utilizing a membrane with a molecular weight cut-off (MWCO) of 1.0 kDa or 3.5 kDa, for more efficient purification [73]. In contrast, membranes with an MWCO of 0.5–1.0 kDa typically result in only partial removal of by-products over a given period. High speed centrifugation, i.e., subjecting the sample to a centrifugal speed between 8000 and 13000 rpm for several minutes [78], effectively removes coarse impurities, primarily microscopic particles. The supernatant obtained after centrifugation contains the CDs, along with impurities that may include organic molecules (such as carbonization by-products or starting products) or carbon particles of size intermediate between the CDs and insoluble aggregates.

For instance, Essner et al. [79] investigated the impact of dialysis on the quality of CDs. Syntheses were conducted using a two-step hydrothermal and microwave-assisted approach, where citric acid (carbon source) was combined with urea or ethylenediamine as nitrogen sources. Following synthesis, CDs were purified by dialysis. Careful comparison revealed significant differences in the optical and morphological properties of the dialysate (components transported into the water bath) and retentate fractions (solution remaining inside the dialysis membrane) obtained during dialysis.

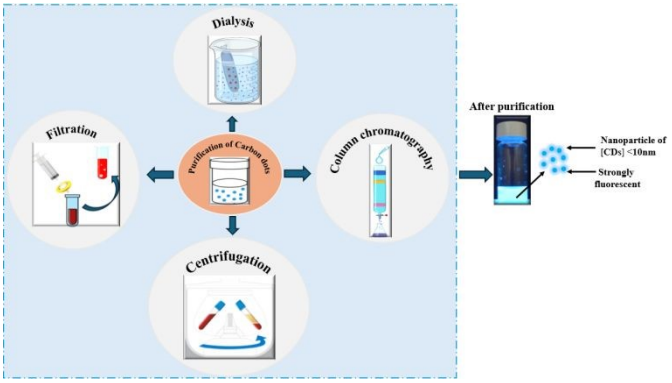

Figure 6. Various methods reported for the purification and separation of CDs.

Table 1. Advantages and limitations of CD synthesis methods.

Methods		Advantages	Limitations	ref.
Top down	Electrochemical/ chemical oxidation	Controllable size, good reproducibility and high purity,	Difficult to control, complex purification process	29,30,80

		process at normal temperatures		
	Laser ablation	Rapid synthesis with controllable morphology and size, absence of harmful chemicals, high purity and good reproducibility	Intricate operation, high cost, low yield, low quantum yield, and constraints for large-scale synthesis.	[35,36,81,82]
	Ultrasonic	Easy operation, eco-friendly high yield, and high quantum yield, products have good stability and no agglomeration at high salt concentrations.	High energy cost, long synthesis	[35,39,83,84]
Bottom up	Hydro/solvothermal	High yield, purity and quantum yield, low cost, good dispersion, diverse starting materials, biomass starting materials, nontoxic, environmentally friendly, well-controlled nucleation processes, properties solvent-dependent.	Long synthesis, harsh conditions, high vapor pressure, unsatisfactory size and morphological uniformity.	[35,45,63,64,66,66,76,85,86]
	Microwave	Easy operation, fast synthesis, uniform size distribution, high quantum yield, easy size control, eco-friendly, biomass	High energy cost	[59,87–89]

View Article Online
DOI: 10.1039/D6TB00190D

		starting materials		
	Pyrolysis	Simple operation, solvent-free, economical, wide precursor tolerance, short reaction time, low cost, suitable for large-scale production, biomass starting materials	Broad non-uniform size distribution, high temperatures required, separation from other molecules challenging.	66,69,70,74,90

4. Properties and Characterization

The variety of preparation methods and the wide range of carbon precursors have contributed to the diversity of structures and compositions of CDs. Nevertheless, CDs reported in different studies often display remarkably similar physicochemical properties. Reference to the literature on carbon dots leads to a multitude of abbreviations other than CD. One finds also CNP (carbon nanoparticles), CND (carbon nanodots), GCD (graphene carbon dots), GQD (graphene quantum dots), CQD (carbon quantum dots) and many others when, for example, heteroatom doping is specified. The use of the word "quantum" in this context is a reference to inorganic Quantum Dots (QDs), suggesting an analogy of CDs with QDs and that in both cases the photoluminescence is due to the quantum confinement effect (QCE).

4.1 Composition, morphology, and surface properties of CDs

The composition and structure of CDs are influenced by the synthesis method, surface defects, dopant atoms, and differences in surface functional groups, and depends strongly on the nature of the precursors and post-synthesis treatments. Since top-down methods start with essentially carbonaceous materials, the resulting CDs tend to be the same, though surface oxygen functions frequently arise or are sought. CDs produced by bottom-up processes are, like their precursors, more heterogeneous and are typically composed of elements such as C, H, O, N, and S. Surface carboxylic acid groups are especially abundant due to the oxidation of organic precursors [74].

The morphology and composition of CDs can be characterized by a multitude of techniques (Figure 7). CDs prepared by bottom-up techniques have diameters (determined by Transmission Electron Microscopy (TEM)) between 1 and 10 nm, tending to peak around 2–3 nm, and are represented as being roughly spherical, whereas CQDs obtained by top-down techniques usually have a better defined layer structure and may well be oblate (a flattened sphere) [91]. Their height, according to Atomic Force Microscopy (AFM), generally lies between 1 and 5 nm [92]. High-resolution TEM observations, along with calculations from X-ray diffraction (XRD) peaks, indicate that the interplanar spacing of graphene-like layers in S,N-CQDs (from feijoa leaves and thiourea by microwave heating) is typically 0.18–0.24 nm, with a graphitic interlayer distance of 0.32 nm [93]. Single-layer graphene quantum dots (S-GQDs) synthesized by the oxidation of coals show a narrow size distribution, with a diameter of about 10 nm (TEM) and an average height (AFM) of about 0.5 nm. A broad XRD peak around 25° was attributed to the (002) planes of graphite [94]. Raman spectra displayed two characteristic peaks corresponding to the out-of-plane stretching mode of sp^2 defects (D band) and the in-plane stretching mode of sp^2 hybridized carbon (G band) [94]. X-Ray Photoelectron Spectroscopy (XPS) spectra presented three main peaks, associated with C–C, C–O, and C=O carbon atoms, and Fourier Transform Infrared (FTIR) spectra confirmed the presence of various functional groups on the surface of CDs, with peaks for C=C, C=O, C–O, and O–H groups [94]. CNPs prepared by nitric acid treatment of candle soot are predominantly composed of amorphous or nanocrystalline sp^2 carbon clusters [95], while CNPs obtained by laser ablation of graphite powders show the presence of sp^3 hybridized carbon structures, as well as C–O and C=O vibrations, characteristic of –COOH groups [96].

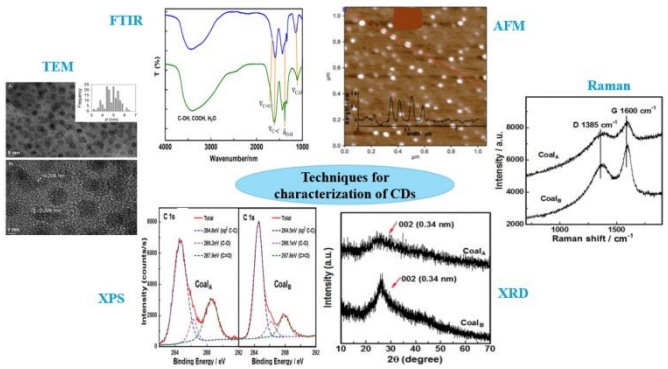

Figure 7. Techniques for the characterization of CDs. Reproduced from ref. 91 with permission from American Chemical Society, copyright© 2009 and reproduced from ref. 94 Royal Society of Chemistry, copyright© 2014.

4.2 UV-Visible absorption spectroscopy

Different carbon precursors and synthetic methods lead to CDs with varied absorption behaviors. Conjugated π-electrons of the sp^2 hybridized structures in CDs absorb in the ultraviolet at 260−320 nm [97] or 230–320 nm [98], with tails that extend into the visible; the wavelength may increase upon surface passivation [97]. For the carbon core, the substantial absorption peak at 230 nm is primarily due to π-π* transitions of aromatic C−C bonds, while the shoulder at around 300 nm is attributed to n-π* transitions of C=O bonds or other functional groups [98]. Carbon nanoparticles (CNPs) prepared from different ratios of urea to citric acid by microwave synthesis have diverse absorption and emission properties: CNP1, urea/citric acid = 0.2 (Figure 8b); broad absorption peak at 336 nm; CNP2, urea/citric acid = 2 (Figure 8c); maximum at 420 nm [99]. Supra-carbon nanodots (supra-CNDs) were obtained by aging urea/citric acid CNDs. While CNDs had a single absorption band at 340 nm, supra-CNDs, in addition to an absorption peak at 356 nm, exhibited a well-defined strong absorption at 700 nm, covering the visible to NIR range of 470–1000 nm (Figure 8a) [100]. Near Infrared (NIR)-absorbing nanodots, including carbon-based and conjugated polymer systems, are capable of converting light into thermal or acoustic energy, and are thus widely applied in photoacoustic tumor imaging and photothermal therapy [101].

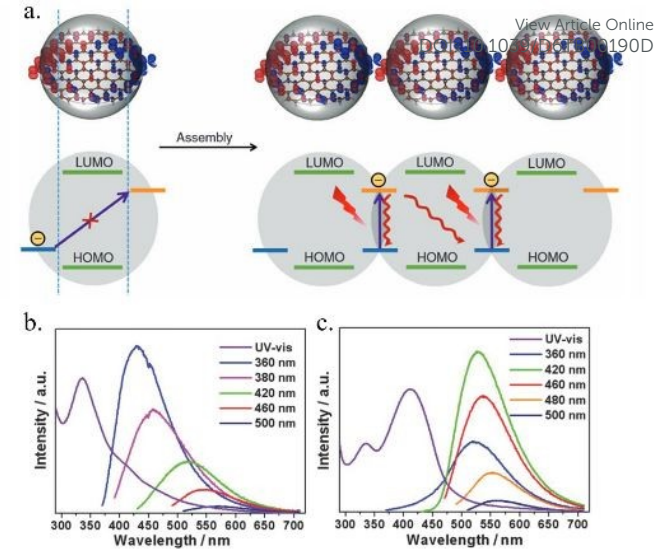

Figure 8. (a) Schematic of supra-carbon nanodots (CNDs) showing the energy level alignment and photothermal conversion mechanism. Reproduced from ref. 100 with permission from Springer nature, copyright© 2016. Blue horizontal bars represent the ground state or Highest Occupied Molecular Orbital (HOMO) level ("a" level), while yellow horizontal bars indicate the excited state or Lowest Unoccupied Molecular Orbital (LUMO) level ("d" level). Jagged red lines depict NIR irradiation leading to electron excitation, and wavy red lines indicate heat generated from non-radiative relaxation of these excited electrons. (b) Comparative UV-Vis absorption and photoluminescence (PL) spectra of CNP1 and (c) CNP2 in ethanol/water. Reproduced from ref. 99 with permission from WILEY-VCH Verlag GmbH & Co. KGaA, Weinheim, copyright© 2013.

4.3 Photoluminescence

By absorbing photons with energies greater than the bandgap, electrons transition from the valence band to the conduction band, thus attaining an excited state. Upon returning to the valence band, energy is emitted in the form of photons as the electrons return to the ground state [102,103]. Most CDs emit blue or green light, but some emit at longer wavelengths, potentially covering the entire visible spectrum. CDs generally display broad emission spectra and excitation-dependent fluorescence (i.e., emission wavelength and intensity change with excitation wavelength), which have potential for application in multicolor imaging [95,104].

The fluorescence exhibited by CDs is one of their most intriguing characteristics, and has been extensively investigated and

View Article Online
DOI: 10.1039/D6TB00190D

documented [105]. Compared to traditional organic/inorganic photoluminescent materials, CDs have very good photostability and resistance to photobleaching. They can be stored in air at room temperature for extended periods without their fluorescence properties changing and conserve over 90% of their original intensity after several hours of UV irradiation [106,107].

The likelihood of CDs transitioning from the excited state back to the ground state through fluorescence radiation defines the quantum yield (QY), an highly important metric [108]. In early work, the QY of CDs was relatively low (generally less than 10%), but it can be significantly enhanced by surface passivation or heteroatom doping (see below). These modifications alter the surface structure, energy levels, and emission traps of the CDs, thereby improving their fluorescence performance and possibly shifting the emission peak positions [92]. For example, CDs synthesized by laser ablation and treated with organic and polymeric passivators exhibit multicolor fluorescence, covering visible to NIR wavelengths, attributed to the stabilization of surface traps by the passivating agents [109]. Other factors influencing the fluorescence properties of CDs are the type of solvent, solution pH, temperature, and concentration. For instance, deep red-emissive carbonized polymer dots (CPDs) with long-wavelength emission and a narrow full-width-at-half-maximum (FWHM ~20 nm) have been developed by selecting nitrogen-rich polymeric precursors and precisely controlling the reaction temperature, which governs the degree of carbonization and the formation of π-conjugated structures responsible for their optical properties [110]. When GQDs, obtained solvothermally from graphene oxide, are dissolved in different solvents such as tetrahydrofuran, acetone, dimethylformamide (DMF), and water, there is a notable shift in the emission peak from 475 nm to 515 nm. The different solvents affect the surface emission traps or energy levels of the CDs, thereby altering the emission wavelength [111]. The fluorescence response of N-doped CDs obtained from alginic acid and ethanediamine is notably pH-dependent. The fluorescence intensity of these N-doped CDs notably decreases as the solution pH is adjusted from 2 to 13, yet the emission peak position remains unchanged [112]. For CDs synthesized from a silane coupling agent KH-602 and citric acid, when the pH increases from 1 to 12, the fluorescence intensity rises steadily to a level almost five times that at pH 1. Moreover, the emission peak blue-shifts, moving from 520 nm to 463 nm under the same excitation conditions [113]. The pH-dependent fluorescence of CDs arises from the protonation and deprotonation of surface functional groups such as –COOH, –OH, and $–NH_2$, which influence the electronic structure by altering the surface charge distribution and shifting the Fermi level [114].

4.4 Up-conversion fluorescence

The up-conversion fluorescence observed in CDs refers to an optical process in which the emission occurs at a shorter wavelength than the excitation light, contrary to conventional fluorescence. This behavior is primarily attributed to multiphoton excitation mechanisms, where two or more photons are absorbed before photon emission, as demonstrated by Cao et al. [115] in their study on CDs for multiphoton bioimaging. Additionally, Shen et al. [116] proposed that specific electronic transitions, involving excitation of π-electrons to higher energy orbitals followed by relaxation to σ-orbitals, could also account for the up-conversion behavior in graphene quantum dots. However, Wen et al. [117] highlighted the possibility of experimental artifacts, such as second-order diffraction at λ/2, which may falsely appear as up-conversion and can be mitigated by applying suitable optical filters. Zong et al. [118] provided deeper insights into the photoluminescent behavior of CDs, helping to clarify how these materials emit light under various conditions. Their findings reinforced the overall understanding of the optical properties of CDs, including phenomena such as excitation-dependent emission and potential up-conversion luminescence. These unique up-conversion characteristics make CDs highly attractive for applications in bioimaging, photocatalysis, and optical data encryption, particularly due to the low phototoxicity of IR and NIR photons used for excitation [119,120].

This was further explored by Lu et al. [121], who found that carbonized polymer dots from o-phenylenediamine and dopamine show two-photon emission under 800 nm femtosecond pulse laser irradiation. Certain CDs, such as those obtained by ultrasonication using citric acid, graphene oxide, fluoresce at 300–600 nm upon excitation at 650–1000 nm [118,122,123]. The up-conversion properties of CDs are not only utilized in bioimaging but also in sensors. For example, the quenching effect on the up-conversion fluorescence of CDs from fresh pepper and H_2O by hydrothermal method 180 °C for 5 h, under 780 nm excitation was used to establish a method for detecting ClO^- in water samples [124]. Moreover, the up-conversion properties of CDs are employed in novel photocatalytic composites, by combining them with wide-bandgap semiconductors to convert long-

View Article Online
DOI: 10.1039/D6TB00190D

wavelength light into short-wavelength light, improving photocatalytic efficiency [125,126].

4.5 Biocompatibility

Unlike semiconductor QDs such as CdSe and CdS, which contain toxic heavy metals, CDs are a new type of carbon-based fluorescent nanomaterial with low cytotoxicity and high biocompatibility [127–130]. CDs synthesized by microwave pyrolysis of citric acid and ethylenediamine show extremely low toxicity towards mouse fibroblast cells (L929), with high cell viability even at concentrations up to 6 mg mL^{-1} [131]. Further experiments, including studies on HeLa cells, showed that these CDs have minimal impact even at high concentration. Fluorescence microscopy revealed that the cells not only maintained good morphology but also had a strong blue fluorescence [132]. Animal studies have confirmed the low in vivo toxicity of CDs [86,133]. When injected intravenously into mice, CDs did not provoke any significant toxic responses or inflammatory symptoms and were rapidly excreted via the renal and hepatic systems [134,135]. Similarly, studies have shown that CDs produced via an alkali-assisted ultrasonic route using glucose are non-toxic even at high concentrations, exhibiting excellent biocompatibility across different cell lines, including cancerous and non-cancerous cells [136].

CDs undergo photodegradation or generate reactive oxygen species (ROS) upon exposure to laser radiation [137]. Degradation of the carbon core structure leads to the production of electrons and point defects. Consequently, hydroxyl and alkyl radicals can be generated, and these may damage biological entities. This distinctive property has resulted in the widespread use of functionalized CDs in biomedicine. Although CDs generally exhibit low toxicity, their surface functionalization may alter their biocompatibility. For instance, CDs bearing specific ligands can be used to label and track cells, but it is important to note that the ligands may influence the interactions between the CDs and cells [72]. Furthermore, studies have shown that the charge on CDs plays a significant role in their biocompatibility. In general, CDs with neutral or negative charges are the less toxic [138,139].

5. Modulation of fluorescence properties

5.1 Quantum size effect and size control techniques

Carbon dots (CDs), typically ranging from 1 to 10 nm in size, exhibit quantum confinement effects (QCE) due to the spatial restriction of electrons within their nanoscale structure. This confinement leads to quantized energy levels, resulting in size-dependent optical properties, such as tunable fluorescence emission [140]. These quantum size effects also enhance their photochemical stability, electronic transitions, and catalytic activity, making them promising for sensing, imaging, and optoelectronic applications [141,142].

Yellow fluorescent GQDs were prepared from carbon black by acid-assisted exfoliation. Coating with polyethyleneimine (PEI) of different molecular weights gave blue- (monocoated, MW 1800 Da) and red-emitting (polycoated, MW 600 Da) GQDs [143]. GQDs, obtained from carbon nanofibers by acid breakdown and chemical exfoliation, are of the order of a few nm in size. Their photoluminescence can be tailored by changing process parameters to vary their size [144]. Density functional theory (DFT) and time-dependent DFT have been employed to explore the influence of size, edge states, and shape on the bandgap and fluorescent emission of CDs [145]. By thermal treatment of triphenol, triangular CDs with multicolor emission were synthesized, and their size was adjusted to control the emission wavelength and QY [146]. In another study, thiourea and p-phenylenediamine were used as precursors and the reaction solvents were varied to produce CDs with blue, green, and red emissions. Subsequent DFT calculations shed light on how the sp^2 domains regulate the emission wavelengths. An increase in the size and the introduction of amide bonds leads to a corresponding increase in the size of the sp^2 domains, resulting in a red-shift in the emission [147]. Thus, adjusting the size of CDs offers a promising approach to control their luminescent properties, notably for the fabrication of CDs with longer emission wavelengths.

The template/carrier synthesis method is an effective way of controlling the size of the product. Typically, the process involves two key steps. Initially, mesoporous materials or silica spheres are employed as the template, and CDs are synthesized by calcination at high temperature. The template acts as a carrier, limiting the growth of CDs and preventing their aggregation, which effectively controls their size. Subsequently, the template is etched away to release the CDs, ensuring they are free from constraints and aggregation. This method ensures precise control over the structural characteristics of the CDs. Liu et al. created F127-silica composites as templates by grafting F127, an amphiphilic polymer, onto nano-silica spheres [148]. A soluble phenol-formaldehyde resin was polymerized onto the composite, and the material was then carbonized under argon, resulting in a CD/silica composite. Etching away the silica template

View Article Online
DOI: 10.1039/D6TB00190D

by sodium hydroxide solution left 1.5~2.5 nm-diameter CDs. After PEG1500N passivation, they fluoresced strongly and their maximum emission wavelength could be adjusted to 400–580 nm [150]. Four organic molecules with different aromatic frameworks were used as carbon sources to develop a novel soft-hard template method for the synthesis of CQDs with tunable size, composition, crystallinity, and photoluminescence properties. Mesoporous silica (OMS) SBA-15 and a copolymer (Pluronic P123) were used as the hard and soft templates, respectively [149]. Generally, CDs obtained by the template method are uniform in size, which can be regulated by modifying the type and quantity of the template or ligand. Nonetheless, the experimental procedure is intricate, and detaching the template poses a challenge. There is a risk of compromising the structural integrity of CDs and modifying their fluorescent characteristics when they are separated from the template.

5.2 Heteroatom doping techniques

Doping is a highly effective method for modifying the physicochemical properties of CDs, and has attracted significant attention in recent years [150]. It involves the incorporation of hetero-atomic organic precursors or metal ions into CDs. This process aims to enhance QY, modulate light waves based on the dopant atom, and broaden functionalities and applications. Doping can be divided into two main categories: non-metallic atom doping and metal atom doping [151]. In so far as non-metallic atom doping involves the overlapping of atomic orbitals between non-metallic and carbon atoms, it can alter the electronic structure, and the nanostructure. On the other hand, metal atom doping can change the electron density distribution and energy gap of CDs, leading to significant modifications in their optical, electrical, and magnetic properties. Metal atoms have more electrons, more empty orbitals, and larger atomic radii than non-metallic atoms.

5.2.1 Doping by Non-Metallic Atoms

Non-metallic atoms, such as nitrogen, phosphorus, oxygen, fluorine, and sulfur, can be incorporated into CDs to modify their electronic structure and introduce structural defects. Among these, nitrogen-doped CDs are the most common. Nitrogen, as a typical electron-rich dopant, improves the fluorescence performance of CDs by injecting electrons and changing their internal electronic environment. For example, Yang et al. examined the bandgap and emission states of GQDs by using boron and nitrogen as electron-deficient and electron-rich dopants, respectively [152]. They synthesized undoped GQDs (U-GQDs), boron-doped GQDs (B-GQDs), and nitrogen-doped GQDs (N-GQDs). Compared to U-GQDs, B-GQD fluorescence was red-shifted, while N-GQDs displayed a blue-shift. In B-GQDs, boron atoms provide vacant orbitals for the carbon π-system, resulting in an increase in the energy level of the HOMO. Conversely, in N-GQDs, pyridine nitrogen contributes an electron pair to the occupied π-orbitals, leading to a decrease in the HOMO energy level and an increase in the bandgap. For instance, N-CDs, synthesized by microwave pyrolysis of glucose and amino acids, gave a high QY of 69%. The emission wavelength of CDs can be adjusted by varying the amount of nitrogen doping [153]. Highly doped N-CDs were prepared by microwave-assisted pyrolysis of chitosan, acetic acid, and ethylenediamine. N-doping enhances the surface defects of CDs, thereby improving their QY [154]. Different types and positions of nitrogen doping significantly influence the absorption and emission behaviors [155]. According to the study, central doping (core) introduces mid-gap states that are non-fluorescent and obstruct the transition channels for photo-excited electrons, thereby reducing fluorescence. In contrast, edge doping (periphery) preserves the π-conjugated system of GQDs, enhancing the radiative transition probability of photo-excited electrons and thus significantly increasing fluorescence intensity. Green and yellow fluorescing P-doped CDs were synthesized from valine and phosphoric acid at 90 °C. The red-shift in fluorescence emission, from green to yellow, demonstrates that the inclusion of phosphorus introduced new electronic states, altering the bandgap of the CDs and leading to significant changes in their electronic structure [156]. N-, S-, and Se-doped CDs were synthesized hydrothermally from Chinese ink with DMF, NaHS, and NaHSe, respectively. The fluorescence emission varied with the electronegativity of the doped heteroatoms: lower electronegativity (S, Se) induced a red-shift, whereas higher electronegativity (N) caused a blue-shift [157]. Novel B-doped CDs, prepared by microwave pyrolysis of citric acid, boric acid, and urea, had a significantly higher non-linear optical response than undoped dots [158]. N,S-co-doped CDs, synthesized from glutathione by a hydrothermal method, had optical properties, stability, water solubility, and a QY of 17.5%, which made them suitable for applications in temperature sensing and as fluorescence sensors for tetracyclines [159]. In N,F-co-doped far-red fluorescent CDs, synthesized solvothermally from citric acid, urea, and NH_4F, the N,F

View Article Online
DOI: 10.1039/D6TB00190D

doping reduces the HOMO-LUMO energy gap, red-shifting the emission [160].

5.2.2 Doping by Metallic Atoms

Metal ion doping modifies the electron density distribution and energy gap of CDs, with consequent changes in their optical, electrical, and magnetic characteristics [161]. Among the commonly employed metal ions for this purpose are Cu, Mn, Zn, Gd, Ge, Tb, and Zr [162] The incorporation of manganese into CDs leads to green [163] orange [164], red [165], and even NIR emissions [166]. Similarly, the addition of lanthanide compounds as dopants produces distinctive narrow fluorescence emission peaks. For example, ytterbium-doped CDs have notable peaks at 998 nm, while neodymium-doped CDs peak at 1068 nm [161]. Metal doping of CDs not only enhances their inherent fluorescence properties but also imparts unique attributes associated with metals. Gadolinium- [167], manganese- [168], iron- [169], and nickel-doped [170] CDs have been employed in magnetic resonance imaging because of their exceptional imaging performance and biocompatibility. Furthermore, CDs doped with metal ions have catalytically active centers that can modify their electronic structure and chemical reactivity in photo-, electro- and chemical catalysis. For example, the yield of the photo-oxidation of 1,4-dihydro-2,6-dimethylpyridine-3,5-dicarboxylate is 3.5 times higher with Cu-CDs than with undoped CDs. This increase in yield is attributed to changes in the electron supply and acceptance capabilities of CDs by the copper ions [171]. However, it is imperative to evaluate the potential toxicity of metal ions prior to their usage, as these aspects can significantly affect the biological applications and environmental safety of CDs.

5.3 Surface passivation and functionalization

In order to enhance the performance and stability of CDs in various applications, chemical modification of the surface and coating treatments are often employed [172,173]. By the use of silanes, polymers, or other organic materials as coating agents, CDs can be protected against photobleaching and chemical degradation, while also being functionalized to introduce specific chemical groups or biomolecules [174]. This expands their potential applications in areas such as biomarkers, drug delivery, and environmental monitoring. Modification of the surface properties of CDs, synthesized by the hydrothermal oxidation of graphite, by means of aminophenylboronic acid improved the QY from 3% to 50%. At the same time the fluorescence emission peak blue-shifted from 435 nm to 370 nm. These modified CDs can be used to selectively detect glucose [175]. Carboxyl groups present on the surface of CDs were coordinated with Tb^{3+}, to establish a fluorescence detection method for *B. anthracis*, capitalizing on their strong binding affinity for Tb^{3+} [176]. Passivating the surface of CDs decreases non-radiative recombination and significantly enhances their QY. By the use of I1500N and PEG-200 as passivators, CDs with a QY as high as 75% were obtained [177]. CDs with enhanced fluorescence intensity were prepared by microwave-assisted pyrolysis of sugars, PEG-200 being used as passivating agent [178]. Apart from using PEG as a passivating agent, other viable options include polyethylenimine (PEI) [179] and various small amine molecules, such as 4,7,10-trioxa-1,13-tridecanediamine [180], ethylenediamine [181], and ethanolamine [182]. The QY of passivated CDs was significantly enhanced by amide bond formation and ethylenediamine grafting [183]; the surface polarity of the CDs could be controlled by adjusting the length of the hydrocarbon chain of the amine. Similarly, the fluorescence of aniline-passivated GQDs not only shifted from blue to white - where white fluorescence refers to a broad emission spectrum covering multiple visible wavelengths - but their surfaces went from hydrophilic to hydrophobic. This change in surface properties allowed these GQDs to be uniformly dispersed in a poly(3-hexylthiophene-2,5-dialkyl) matrix [184]. CDs produced by oxidation methods typically have oxygen-containing surface functional groups, which can be chemically reduced in order to enhance and/or shift their fluorescence. For example, sodium borohydride can reduce green-emitting CDs to blue-emitting CDs, increasing their QY [184]. These reduced CDs can be reoxidized back to their original green luminescent state, enabling repetitive redox cycling. Moreover, alternative reduction pathways, such as hydrothermal treatment [185], hydrazine reduction [186], and UV irradiation [187], have also been found to alter the surface oxygen-containing groups and fluorescence characteristics of CDs.

6. Applications in Heavy Metal Assay

Due to their exceptional optical properties and stability, CDs have considerable potential for the detection of metal ions. In the context of wastewater treatment by composites [188,189], CDs may be employed as fluorescent probes to identify metal ions. Their photoluminescence properties are adjustable, and they exhibit multicolor emission characteristics dependent on the excitation wavelength. Moreover, the functional groups located on the surface

View Article Online
DOI: 10.1039/D6TB00190D

of CDs, including amino, carboxyl, and hydroxyl groups, can interact with metal ions, thereby altering the electron transfer path and leading to either fluorescence quenching or attenuation [190,191]. Fluorescence detection of CDs typically involves various mechanisms, such as static quenching, dynamic quenching, resonance energy transfer (FRET), photo-induced electron transfer (PET), surface energy transfer (SET), Dexter energy transfer (DET), and the inner filtering effect (IFE) [192,193] (Figure 9). Consequently, the fluorescence intensity of CDs can serve as a means of detecting minute quantities of metal ions within the environment. CDs, functioning as fluorescent probes, offer advantages such as rapidity, high efficiency, strong selectivity, cost-effectiveness, and environmental friendliness.

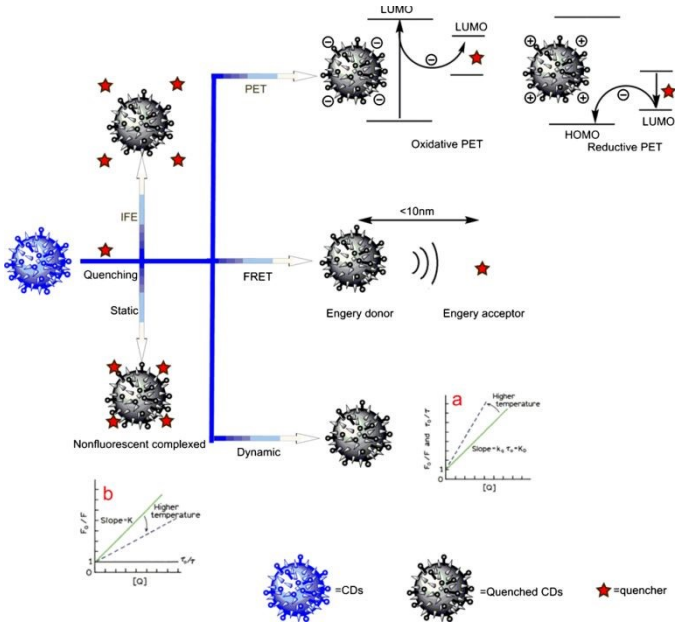

Figure 9. Quenching mechanisms of CDs used for detecting analytes. Reproduced from ref. 192 with permission from Springer Nature, copyright© 2017.

6.1 Hg^{2+} Determination

Traditional mercury ion detection methods, such as atomic absorption and electrochemical methods, although effective, are often limited by the requirement for expensive equipment and complex operation procedures. In contrast, because of their optical properties, CDs have become an ideal choice for detecting Hg^{2+}. In 2012, a study reported for the first time the use of CDs as fluorescent sensors for the detection of Hg^{2+} [194]. These CDs, prepared by pyrolysis of EDTA, exhibited strong fluorescence due to radiative exciton recombination. In the presence of Hg^{2+}, fluorescence was quenched via non-radiative electron–hole recombination facilitated by charge transfer between Hg^{2+} and surface functional groups. Upon addition of biothiols such as cysteine, which bind Hg^{2+} through strong Hg–S interactions, the metal ions were displaced from the CD surface, leading to fluorescence recovery. This reversible "off–on" response enabled label-free and selective detection of both Hg^{2+} and biothiols in aqueous solution. Fluorescent CDs, which can detect Hg^{2+} with a linear range of 10–50 µM and a LOD of 3 nM, have been synthesized from strawberry juice [195]. An economical hydrothermal synthesis of nitrogen-doped, 4.5 nm-diameter CQDs from folic acid has been reported [196]. Excited at 470 nm, they emit at 390 nm and have a strong response to Hg^{2+} ions. They can be used as a fluorescent sensing platform for label-free and sensitive detection of mercury, even in the presence of other ions, with a detection limit of 0.23 µM. 'On-off' type fluorescent sensors have been developed in other studies. Hg^{2+} ions can quench the fluorescence of N-doped CDs (N-CDs) in selective metal-ion detection experiments [197] (Figure 10a), and the addition of glutathione (GSH) to the mixture of Hg^{2+} and N-CDs gradually restores the blue fluorescence, based on which a 'turn-off-on' fluorescence Hg^{2+} ion sensor was constructed. Hg^{2+} can quench the fluorescence of blue fluorescent CDs [198], while iodide ions can restore it, leading to a 'turn-off-on' detector for mercury and iodide ions at the same time, with good selectivity and recovery. This Hg^{2+} ion sensor was applied to tap water and real lake-water samples. Li et al. prepared blue-emitting, 7–11 nm-diameter GQDs with a QY of 15% from citric acid (200 °C, pH 8) [199] (Figure 10b). These were capable of detecting Hg^{2+} in water by charge adsorption-induced fluorescence quenching (92% quenching efficiency) with a LOD of 0.44 nM and a linear range of 1–50 nM. Fluorescence recoveries of 91–95% from lake-water samples were achieved. N-doped, 1.0–3.5 nm-diameter CDs, prepared by a one-step electrochemical method from sodium citrate and urea, had a LOD of 3.3 nM for Hg^{2+} in water and could detect Hg^{2+} in spring, tap and lake-water [200]. The excellent sensitivity and selectivity of this stable, inexpensive carbon material make it suitable for monitoring Hg^{2+} in environmental applications.

View Article Online
DOI: 10.1039/D6TB00190D

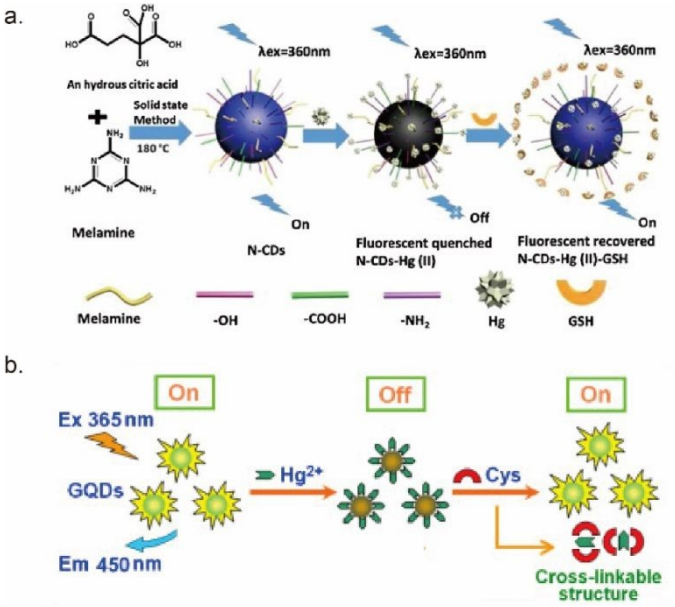

Figure 10. (a) Formation of N-CDs, the binding of N-CDs with Hg^{2+} and GSH, and quenching off-on N-CDs by Hg^{2+} and GSH. Reproduced from ref. 197 with permission from Elsevier B.V., copyright© 2017. (b) Analytical pathway for Hg^{2+} and cysteine by fluorescence switching of GQDs. Reproduced from ref. 199 with permission from Elsevier B.V., copyright© 2014.

6.2 Cu^{2+} Determination

Copper is one of the essential trace elements and plays a key role in regulating physiological activities. However, excessive intake may cause serious neurological disorders such as the hair-twisting syndrome and hepatomegaly [201]. According to the standards of the US Environmental Protection Agency, human intake of copper ions should not exceed 1.3 mg L^{-1} [202]. Therefore, the development of fluorescent CD probes for the detection of copper ions in the environment and in living organisms has become extremely important. A fluorescent probe for intracellular Cu^{2+} detection has been developed by integrating an organic molecule, N-(2-aminoethyl)-N,N,N'-tris(pyridin-2-ylmethyl)ethane-1,2-diamine, which has a specific response to Cu^{2+}, into a composite system consisting of carbon and CdSe/ZnS quantum dots [203]. This probe not only showed high sensitivity (LOD, 1 μM), but also excellent photostability. In a more recent study, red dual-emissive CDs [204] were synthesized solvothermally from l-glutamic acid, o-phenylenediamine and urea as precursors. These CDs were used for ultrasensitive ratiometric detection of Cu^{2+} by monitoring the intensity ratio of fluorescence emission peaks at 605 and 650 nm (F_{605}/F_{650}), achieving a LOD of 0.59 nM in vitro. The system showed good stability, low cytotoxicity, and allowed real-time monitoring of Cu^{2+} dynamics in living cells and tissues. CD-modified silver nanoparticles (CDs-AgNPs) were prepared by reducing $AgNO_3$ in the presence of CDs obtained by microwave heating of citric acid and ethylenediamine [205] (Figure 11a). Based on the strong interaction between the functional groups of the CDs and Cu^{2+}, a simple, sensitive (LOD, 0.04 μM) and highly selective Cu^{2+} sensor was developed. In a more advanced application, spherical P-doped CQDs (P-CQDs) were prepared from trisodium citrate and phosphoric acid with H_2O_2 as an auxiliary reactant [206] (Figure 11b). P-CQDs acted as a solid-state sensing platform for the detection of Cu^{2+}, with a LOD of 0.27 nM. CDs, prepared from polyethylenimine (PEI) by microwave radiation, were used as fluorescent probes for Cu^{2+} detection in animal cells [207]. Their fluorescence intensity varied linearly with the Cu^{2+} concentration in the 0.01–2 μM range, with a LOD of 6.7 nM and good selectivity. This study, along with the work of Wei et al., who prepared CDs from hexadecylamine [208], suggests that Cu^{2+} binds to ammonium groups on the surface of CDs, leading to the splitting of their d-orbitals. This binding creates an electron transfer pathway from the excited state of CDs to the d-orbitals of Cu^{2+}, facilitating non-radiative recombination of electron-hole pairs. Consequently, the radiative transition process is inhibited, resulting in fluorescence quenching.

Although these studies provide efficient solutions, the sensitivity of certain CDs for detecting Cu^{2+} still needs improvement, and the response time needs to be shortened. Some CDs require complex post-processing for purification. Only a very few CDs are currently available as thin films for real-time Cu^{2+} monitoring [209,210].

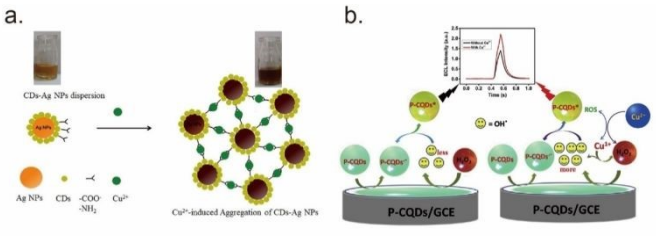

Figure 11. (a) Cu^{2+} recognition mechanism by the colorimetric sensor. Reproduced from ref. 205 with permission from Elsevier B.V., copyright© 2017. (b) Schematic representation of ECL signals generation by P-CQDs-H_2O_2 system and effect of Cu^{2+} ion. Reproduced from ref. 206 with permission from Elsevier Ltd, copyright© 2019.

View Article Online
DOI: 10.1039/D6TB00190D

6.3 Fe^{3+} Determination

Iron is an essential trace element that plays a key role in oxygen metabolism and electron transfer in all organisms. Both deficiency and excess of Fe^{3+} will disturb the in vivo homeostasis of cells. Lack of iron will lead to iron-deficiency anaemia, bronchiectasis and other diseases, while excess Fe^{3+} will cause methemoglobinemia, cirrhosis, osteoporosis, toxic effects and even epilepsy [211]. For the detection of iron ions, CDs serve as fluorescent sensors and offer several advantages: rapid and efficient performance, eco-friendliness, and straightforward operation. When Fe^{3+} ions interact with surface functional groups of CDs, such as carboxyl and hydroxyl, they can affect the electron transfer process, leading to fluorescence quenching, upon which Fe^{3+} detection methods are based. For example, phenol-containing CDs have high sensitivity and selectivity for Fe^{3+}. The surface phenolic hydroxyl coordinates with Fe^{3+}, which facilitates electron transfer and fluorescence quenching [212]. Fluorescent CDs prepared from bergamot by a hydrothermal method [213] show a low LOD (0.075 nM) for Fe^{3+}. CDs synthesized from three types of amino acids recognize mixtures of Fe^{3+}, Hg^{2+} and Cu^{2+}, broadening the range of CD sensor application [214] (Figure 12a). CDs terminated with carboxylates, obtained by pyrolysis of citric acid, show high selectivity and response to Fe^{3+} in different buffer systems [215]. CDs, prepared from o-phenylenediamine and gallic acid (GN-CDs), with dual emission peaks and quenching at 570 nm allowed proportional Fe^{3+} detection with a LOD of 16 nM [216]. Moreover, the quenching induced by Fe^{3+} can be reversed by pyrophosphate. By means of masking agents, differential detection of Fe^{3+}, Cu^{2+} and Ag^{+} was achieved with high-QY CDs synthesized by a ultrasonic method using 1,3,6-trinitropyrene and thiourea [217] (Figure 12b). This method not only showed high selectivity but also provided a means of accurately identifying mixed metal ions.

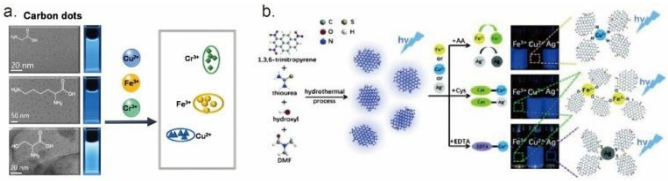

Figure 12. (a) Three kinds of CDs with various surface states synthesized with different amino acids. Reproduced from ref. 214 with permission from Elsevier B.V., copyright© 2016. (b) Preparation of N,S-GQDs and detection of Fe^{3+}, Cu^{2+} and Ag^{+} ions. Reproduced from ref. 217 with permission from Royal Society of Chemistry, copyright© 2017.

6.4 Pb^{2+} Determination

Lead is a highly toxic heavy metal that can accumulate in the body and pose a serious threat to human health. According to the World Health Organization, the maximum tolerable contamination level of Pb^{2+} in drinking water is 10 mg L^{-1}. Excessive levels of lead in the blood can lead to kidney dysfunction and impair brain development, especially in children [218]. Therefore, it is important to trace Pb^{2+} in environmental and water samples. In 2007, Ying et al. reported a method to detect Pb^{2+} using glutathione-modified CdTe and ZnCdSe QDs, with a LOD of 20 nM. Glutathione binds to Pb^{2+} in solution and removes it from the QD surface, causing defects and fluorescence quenching. However, Ag^{+} and Cu^{2+} ions also cause similar quenching, interfering with Pb^{2+} detection [219]. Unmodified CDs (from kerosene soot, refluxed with 240 mL HNO_3 at 125 °C for 72 h) have been developed as novel, eco-friendly fluorescent probes for detecting Pb^{2+} in water [220]. About 50 nm in diameter, they display pH-sensitive yellowish-green fluorescence under UV light. The detection method involves a 'turn-off' fluorescence response when exposed to Pb^{2+}, with good linearity at concentrations from 0.5 to 11 µM and a LOD of 2 nM; the method is highly selective in the presence of 18 different ions. A similar study was conducted on CDs derived from *Ocimum sanctum* leaves [221]. They showed excellent selectivity towards Pb^{2+} ions, with a LOD of 0.59 nM and a linear detection range of 0.01–1.0 µM. This can be attributed to the high binding affinity between the $-NH_2$ group on the surface of these CDs and the empty d-orbital of Pb^{2+}. Pb^{2+} captures the electron pair from the amine nitrogen atom, quenching the fluorescent signal through non-radiative electron transfer. The practical application of these CDs for detecting Pb^{2+} ions was demonstrated in both triple-negative breast cancer cells and real water samples. To enhance the sensitivity and reduce interference in detecting Pb^{2+}, a novel approach using citric acid-based CDs, modified with ethylenediamine and amino acids such as cysteine, histidine, lysine, or arginine, has been developed [222]. The derivatization of CDs by various amino acids modulates their electronic properties, leading to tunable selectivity for detecting metal cations by fluorescence quenching in aqueous solutions around pH 7. Excited at 345 nm, these CDs fluoresce at 450 nm, with the intensity decreasing in inverse proportion to the metal cation concentration (LOD, 8.8 µg L^{-1} for Pb^{2+}).

6.5 Cr^{6+} Determination

Due to its serious carcinogenic and mutagenic properties, the prompt identification of Cr^{6+} is considered essential. CDs have been prepared

View Article Online
DOI: 10.1039/D6TB00190D

from diverse carbon sources by various methods for Cr^{6+} detection [223–225]. CDs prepared hydrothermally from animal hair have remarkable water solubility and fluorescence stability, and were used as a probe for the detection of Cr^{6+} in aqueous solution [226]. Fluorescence intensity correlated with the Cr^{6+} concentration of 0.05–100 μM, but with poor selectivity. To reduce the interference caused by other cations, potassium thiocyanide was used to chelate Ag^{+}, and ethylenediaminetetra-acetic acid for Fe^{3+} and Hg^{2+}. Cr^{6+} interacts with oxygen-containing functional groups on the CD surface, resulting in electron transfer: Cr^{6+} is reduced to Cr^{3+}, which leads to non-radiative recombination of electrons and holes, quenching the CD fluorescence. Ruiz et al. used a CD-nylon membrane to detect Cr^{6+} in water with a broad detection range and a LOD of 190 nM [227]. The membrane can be reused after a straightforward water wash. N-doped CDs, synthesized from ground nuts by the hydrothermal method, show a significantly higher QY (18%) than undoped CDs (8%), and are exceptionally selective for detecting Cr^{6+}. The fluorescence quenching caused by Cr^{6+} is reversed by the addition of humic acid and glutathione, allowing an 'off-on' type sensing mechanism. Moreover, the N-CDs were less cytotoxic at higher concentrations, making them suitable for bio-imaging applications in MCF-7 cells [228]. While many CDs are able to detect Cr^{6+} in water, their selectivity for this particular ion is often compromised by the abundance of functional groups on their surface. To address this limitation and enhance the selectivity of CDs towards Cr^{6+}, the incorporation of masking agents and N-doping have been explored [229]. Nevertheless, the excessive use of masking agents raises concerns regarding their potential toxicity and carcinogenicity, while doping necessitates intricate post-processing steps that can significantly diminish the sensitivity of CDs to Cr^{6+}.

Table 2. Summary of optical sensors for various heavy metal ions using carbon dots.

Heavy metal	Material	Analysis range (μM)	Limit of detection (μM)	Linear correlation coefficient	Year	Ref.
UO_2^{2+}	CDs	0-10	0.020	0.998	2022	230
Hg^{2+}	CDs	0-400	0.90	0.995	2021	198
Cu^{2+}	CDs	0.01–2	0.0067	0.998	2017	207
Pb^{2+}	CDs	0.5-11	0.002	0.994	2015	220
Cr^{6+}	GQD	1-500	0.19	0.989	2016	227
Fe^{3+}	CDs	0.1-100	0.016	0.997	2018	216
Cd^{2+}	PC-CDs	0-70	0.015	0.988	2023	231
Cr^{3+}	MoS_2 QDs	0.1-10	0.08	0.994	2020	232
Co^{2+}	N-CPDs	0-200	0.75	0.995	2023	233
Mn^{2+}	KBN-CDs	5-25	1.2	0.998	2022	234
Al^{3+}	Y-CDs	0-10	0.095	0.995	2023	235
Zn^{2+}	CDs	0.02-5	0.006	0.993	20	236

View Article Online
DOI: 10.1039/D6TB00190D

					23	
Sn^{2+}	N,S-RCDs	0-90	0.017	0.997	2021	237

*Where: KBN-CDs: Kentucky bluegrass N-doped CDs; Y-CDs: yellow emissive CDs; N,S-RCDs: N,S-co-doped red CDs; L-GCDs: L-lysine and L-glutathione CDs; CDs@GQDs: CDs mixed GQDs; PC-CD: pyrene carboxaldehyde-CQDs; MoS_2 QDs: molybdenum disulfide QDs.

7. CD composites

CDs have been identified as a viable option for the analysis of heavy-metal ions in aqueous environments. Nevertheless, their high solubility in water limits their applicability in remediation processes. At present, fluorescent CDs are predominantly employed for detection and assay, rather than for the elimination of harmful metal ions. Consequently, it remains imperative to establish CD-based composites that encompass both analytical and removal capabilities. The development of such advanced materials would significantly contribute to the preservation of the environment [238,239].

7.1. CD-inorganic nanomaterial composites

7.1.1 Metal Oxides

Integrating CDs into metal oxide matrices or attaching them to the surfaces of metal oxide nanoparticles yields CD-metal oxide composites which have improved photocatalytic activity and sensing capabilities. These composites involve zinc oxide (ZnO) [240], copper oxide (CuO) [241], titanium dioxide (TiO_2) [242], and iron oxide (Fe_3O_4) [243,244], amongst others. This integration modifies the properties of the individual components, making such nanocomposites particularly useful in environmental remediation activities like photocatalytic pollutant destruction and chemical sensing. TiO_2 is notable among these for its effectiveness in photocatalytic applications, including air purification and water pollutant degradation, due to its high activity, stable properties, low cost, and lack of toxicity. CD-TiO_2 composites synthesized by hydrothermal-calcination and sol-gel methods are substantially better for photocatalytic water purification than pristine TiO_2, degrading various pollutants like gemfibrozil and levofloxacin under sunlight, due to increased formation of reactive oxygen species and improved charge carrier separation. The uniform distribution of CDs within the TiO_2 matrix enhances the optical and structural properties of the photocatalysts, facilitates pollutant degradation and reduces the formation of toxic by-products [245,246]. In another study, a new adsorbent, magnetic CD-$MnFe_2O_4$, for removing UO_2^{2+} from water was prepared by hydrothermal treatment of citric acid. It combines fluorescence, good adsorption capacity (194 mg g^{-1}), magnetic separation ability, and excellent recyclability while allowing real-time monitoring of the process [247]. A new fluorescent probe, combining amine-modified CDs, obtained by a two-step hydrothermal process from trisodium citrate and ammonia, with a mesoporous superparamagnetic nanoparticle (NCD-Fe_3O_4@mSiO_2), can release bound metal ions and recover its fluorescence, enabling the detection of environmental fluoride. This probe accurately measures fluoride (LOD, 65 nM), has a broad response range, and can be reused up to six times for ion detection and removal [248]. Periodic mesoporous organosilicate composites, embedded with CDs prepared by pyrolysis of citric acid, have a two-dimensional hexagonal structure, high specific surface area, and outstanding ability to adsorb 2,4-dichlorophenol and metal ions, including Hg^{2+}, Cu^{2+}, and Pb^{2+} [249]. They have long-range ordered pore channels and tuneable pore sizes. The surface is covered by one to two layers of CDs, which enhance the maximum adsorption capacity, that for 2,4-dichlorophenol reaching 100 mg g^{-1}, and the partition coefficients for metal ions ranging from 2.6 to 7.4 in the order: $Hg^{2+} > Cu^{2+} > Pb^{2+}$.

7.1.2 Zeolitic Imidazolate and Other Metal-Organic Frameworks

Zeolitic Imidazolate Frameworks (ZIFs), a specific subgroup of MOFs, have attracted considerable attention due to their high surface area and porosity. Studies on CD-MOFs provide valuable insights into their potential applications. He et al. synthesized CD-ZIF-8 composite materials by a two-step method controlling their fluorescence intensity and size by changing the CDs, obtained by microwave synthesis from citric acid and urea, and starting material concentrations [250]. A CDs@MOF composite was synthesized by introducing high-QY CDs, obtained by pyrolysis of N-(β-aminoethyl)-γ-aminopropylmethyldimethoxy-silane and citric acid, into a ZIF-8 growth medium, which permitted the incorporation of CDs directly into the framework [251]. Manganese dioxide was incorporated into a CD-ZIF-8 composite, based on citric acid and ethylenediamine, allowing the detection of ascorbic acid by quenched fluorescence recovery [252]. A novel ratiometric fluorescent sensor was synthesized by a facile one-pot route by encapsulating QDs and CDs from citric acid and diethylenetriamine, with good

View Article Online
DOI: 10.1039/D6TB00190D

fluorescence properties, into ZIF-8. The composite showed good stability and dispersibility in aqueous solution and exhibited excellent sensitivity and selectivity toward Cu^{2+}. The linear range was 5–100 nM and the LOD was 1.53 nM [253]. A hybrid multifunctional adsorbent, combining a magnetic Fe_3O_4 core, carboxymethylcellulose-based CDs and a ZIF-8 shell, enabled uranium detection, separation, and recycling from aqueous solutions [254]. Its maximum uranium adsorption capacity at pH 4 and 298 K was 606 mg g^{-1}, slightly greater than that of the same adsorbent without CDs (565 mg g^{-1}). The photocatalytic reaction rate for methylene blue removal by a novel glucose-based CD-decorated ZIF-8 composite, prepared by a simple impregnation method, is six-fold higher than by ZIF-8 alone. This can be attributed to three factors: effective charge separation, an increase in the number of reactive sites, and an improvement in visible light response [255]. N-doped CDs (N-CDs) derived from coconut shells were integrated by a solvothermal method into MOF-5 [256], resulting in a 3D N-CD/MOF-5 photocatalyst, which notably enhanced photoreduction and reduced Cr^{6+} 2.5 times faster than pure MOF-5. This innovative photocatalyst is not only structurally stable and reusable after multiple tests, but also has enhanced visible-light absorption compared to pure MOF-5, and promotes better electron-hole separation. The N-CDs, functioning as both electron acceptors and photosensitizers, significantly contribute to these improved properties. A Zr-MOF adsorbent, UiO-67, with a 3D flower-on-sheet structure, enhanced by N,S-co-doped CDs from trithiocyanuric acid and ethanediamine (UiO-67/NSC), selectively removes tetracycline from water (adsorption capacity 427 mg g^{-1}) [257]. As a sensor it has a wide range (0.08–20 mg L^{-1}), a low LOD (0.06 mg L^{-1}), and no significant toxic effects on human cells.

The high stability and solubility of 4-nitrophenol makes its removal from industrial and domestic water sources a significant challenge. A heterogeneous ternary nanocomposite, glucose-based CDs/MIL-88B(Fe)/Bi_2S_3 (MIL-88 is an iron-based MOF), is an efficient photocatalyst for the reduction of 4-nitrophenol to 4-aminophenol and for the decomposition of dyes under visible light [258].

7.1.3 Layered Double Hydroxides

Layered Double Hydroxides (LDHs) are a class of bimetallic hydroxides with two-dimensional, charged, hydromagnesite-like layer structures with the general formula $[M^{2+}_{1-x}M^{3+}_{x}(OH)_2]^{x+}[A^{n-}_{x/n}]^{x-}mH_2O$ [259] where M^{2+} is usually Fe^{2+}, Ni^{2+}, Mg^{2+}, Co^{2+}, Zn^{2+} or Cu^{2+}, and M^{3+} is Fe^{3+}, Al^{3+}, etc. LDHs have notable chemical and physical properties, including high stability, excellent catalytic ability, large specific surface areas, low toxicity, and anion exchange capacity [260]. A simple calcination method was used to synthesize layered double oxides (LDO) and layered double oxides/CD nanocomposites (LDO-C) with enhanced adsorption properties. In this process, the LDH is transformed into an LDO, while sodium dodecylbenzene sulfonate (SDBS) carbonizes on the surface, forming CDs in situ. UO_2^{2+} adsorption on LDO and LDO-C was pH-dependent above pH 6 and independent below [261]. The maximum adsorption capacity of LDO-C was 354 mg g^{-1} at pH 5 and 298 K, somewhat higher than for LDO, 238 mg g^{-1}. Analysis by BET, FTIR, XPS, and EXAFS indicated that the better performance of LDO-C was primarily due to a higher surface area and abundant oxygen-containing groups. Furthermore, the direct assembly of N,S-co-doped CDs from sodium citrate and L-cysteine, with abundant oxygen-containing groups on the surface of the positively charged LDHs (N,S-CDs-LDHs) led to highly selective and efficient removal of Ag^{+} and Hg^{2+}, with adsorption capacities of 714 mg g^{-1} and 625 mg g^{-1}, respectively [262]. An environmentally friendly LDH/CDs composite had a high adsorption capacity (maximum uptake, 185 mg g^{-1}) for the anionic methyl blue dye [263]. This is attributed to the synergy of LDH and CDs, involving cooperative contributions of electrostatic attraction and hydrogen bonding. Another multicomponent, recyclable nanocatalyst, CDs/Ag@Mg-Al-Ce-LDH, was assembled by integrating CDs, synthesized from 1,10-phenanthroline and citric acid, and silver nanoparticles (AgNPs) into a cerium-doped magnesium-aluminium layered double hydroxide (Mg-Al-Ce-LDH) matrix [264]. The exceptional catalytic performance of this material in the reduction of 4-nitrophenol and the discoloration of organic water pollutants under ambient conditions is attributed to the synergy between CDs and AgNPs. The Mg-Al-Ce-LDH carrier acts as a co-catalyst, with the cerium ions enhancing charge separation.

7.2. CD-organic nanomaterial composites

7.2.1 Nanocellulose

Nanocellulose (NC), a nanoscale form of cellulose, is extracted from renewable resources and features a three-dimensional dynamic cross-linked network. There are three types: cellulose nanocrystals (CNC), cellulose nanofibers (CNF), and bacterial nanocellulose (BNC) [265]. The nanocellulose chains are rich in hydroxyl groups, enabling modification by esterification, etherification, graft copolymerization,

View Article Online
DOI: 10.1039/D6TB00190D

and cross-linking. By means of specific physical or chemical cross-linking methods CDs can be uniformly dispersed within the nanocellulose matrix, not only enhancing their fluorescence but also improving their stability [266]. The covalent attachment of luminescent CDs, prepared by microwave-assisted pyrolysis of glycerol and 4,7,10-trioxa-1,13-tridecanediamine, to carboxymethylated CNF by the 1-ethyl-3-(3-dimethylaminopropyl)carbodiimide/N-hydroxysuccinimide (EDC/NHS) method produced transparent, smooth, and fluorescent CNF-CDs nanopaper [267], effectively combining the properties of both materials. Such composites can be transformed into hydrogels, aerogels, films, etc. for use in fields such as chemical sensing and water remediation. In one study, CDs from glutathione and citric acid were synthesized in situ and coated onto CNF in a one-step process, preserving the fiber structure [268]. This process produced a CD-CNF composite with a rough, bumpy morphology, characterized by amide bonding that enhanced dimensional and thermal stability. An environmentally friendly aerogel has been developed from CNF grafted onto CDs from PEI and citric acid, as the scaffold [269] (Figure 13a). Filter paper was carboxyl-modified by 2,2,6,6-tetramethylpiperidinyloxy radical (TEMPO)-mediated oxidation and freeze-dried to create a pure CNF aerogel. Amino-modified CDs were prepared hydrothermally. The two components were cross-linked by means of the EDC/NHS method, and then purified and dried to obtain a fluorescent aerogel. Under UV light, it fluoresces bright blue, shows high sensitivity in the detection of glutaraldehyde (1 mg kg^{-1}) in water and can be employed for the detection of NOx and aldehydes.

7.2.2 Hydrogels

A hydrogel, a polymer with a three-dimensional network structure, is formed from hydrophilic macromolecular chains cross-linked by physical and chemical methods. This structure serves as an ideal carrier for CDs, maintaining their dispersion across various environments and preventing fluorescence quenching due to aggregation [270,271]. Non-covalent and covalent interactions between the functional groups on the CDs and those of the hydrogel lead to a composite that combines the functionalities of both materials, thereby extending their application range [272]. For instance, a fluorescent nanocellulose hydrogel has been developed for the detection and adsorption of Fe^{3+} and Pb^{2+} in water. The hydrogel, synthesized from carboxylated nanocellulose and CDs, based on ethylenediamine and citric acid, removed 69% of Fe^{3+} and 98% of Pb^{2+}, with adsorption capacities of 98 mg g^{-1} and 442 mg g^{-1}, respectively [273]. This hybrid system significantly enhances the adsorption of organic compounds, heavy metals, and antibiotics. CD-enhanced hydrogels (CDH) have better fluorescence stability than traditional hydrogels, integrating adsorption, detection, and photocatalytic degradation functionalities, thus minimizing secondary pollution and offering significant advantages in wastewater treatment applications [274]. Citric acid/urea CDs were synthesized hydrothermally [275], and then combined with N-isopropylacrylamide and hydroxymethyl cellulose, with potassium persulfate as the polymerization initiator, to form a gel composite. They absorb in the UV, functioning as a photothermal medium, where light is converted into heat, thereby increasing the temperature of the gel. The hydrogel thus produced can effectively adsorb water pollutants and be used in solar-mediated wastewater purification. N-doped carboxymethyl cellulose CDs (CMH–NCD) (norfloxacin, hydrothermal, 190 °C for 8 h) with dual functionalities were formulated for detecting and adsorbing UO_2^{2+} in nuclear wastewater [276]. It was highly selective for UO_2^{2+}, with an adsorption capacity of 194 mg g^{-1} and over 97% removal. Photothermal heating by the CDs within the hydrogel enhanced the convection and diffusion of UO_2^{2+}, increasing contact with active sites and thereby improving adsorption performance. A multifunctional nanofibrillar cellulose/CD (citric acid and ethylenediamine, hydrothermal, 200 °C for 5 h) hydrogel proved highly effective in adsorbing and photocatalytically degrading Cr^{6+} (maximum adsorption capacity 426 mg g^{-1}) [277]. Cr^{6+} adsorption was enhanced by amino groups on the CDs, while the hydrogel structure improved its photocatalytic properties. Furthermore, electrostatic repulsion between the positively charged Cr^{3+} ions and the similarly charged surface of the material facilitated the desorption of Cr^{3+}. For comprehensive wastewater treatment, including the removal of bacteria and microorganisms, a CDH was developed by cross-linking poly(vinylpyrrolidone) (PVP) with CDs prepared hydrothermally from cysteamine and citric acid (Figure 13b) [278]. Under sunlight, the embedded CDs generate reactive oxygen species that degrade dyes and kill bacteria. Chitosan-based hydrogel beads loaded with GQDs obtainbed by pyrolysis of citric acid and iron oxide, were developed for chlorpyrifos removal from wastewater. They achieved virtually 100% adsorption efficiency under ultrasonic assistance, were reusable over seven cycles, and showed strong potential for industrial-scale applications [279].

View Article Online
DOI: 10.1039/D6TB00190D

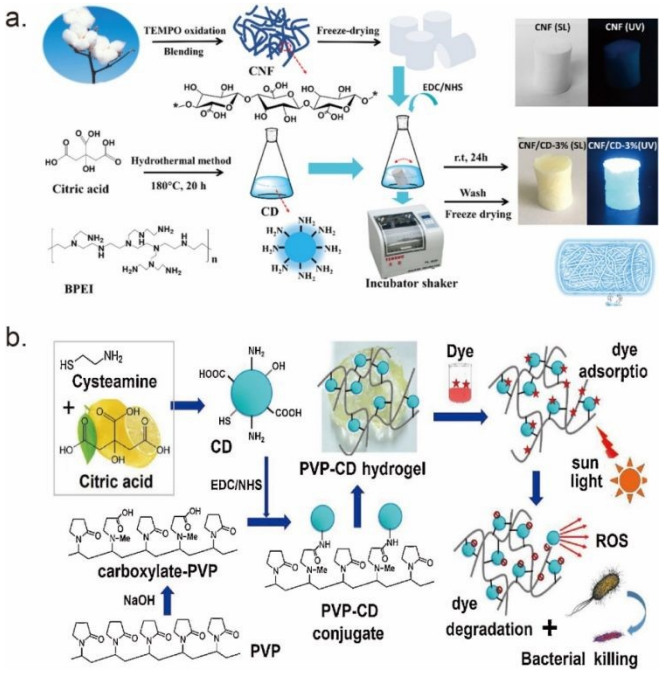

Figure 13. (a) Preparation of CNF/CD-based fluorescent aerogels (SL: under sunlight, UV: under UV radiation). Reproduced from ref. 269 with permission from American Chemical Society, copyright© 2019. (b) Creation of PVP-CD hybrid hydrogel from carboxylated-PVP and CDs for adsorption and photodegradation of dye along with bacterial elimination. Reproduced from ref. 278 with permission from Elsevier B.V., copyright© 2020.

8. Small Molecules of Biomedical Interest

The fluorescence properties of CDs can also be used to detect and assay a certain number of small molecules of biomedical interest. Excess or lack of any of these compounds in the human body leads to a variety of medical conditions, for which reason it is of the utmost importance to have rapid, cheap and portable means of monitoring them.

8.1 Glucose Determination

Glucose, as an indispensable biomolecule in human physiology, serves as a crucial energy source for living cells and is an intermediate product of metabolism [280]. In the bloodstream, the concentration of glucose is typically 3.0–8.0 mM, supporting the normal functioning of bodily tissues. The transport of glucose within the human body has been related to conditions such as diabetes and certain cancers, emphasizing the importance of glucose monitoring for the prevention, diagnosis, and treatment of these diseases. Excessive levels of glucose can lead to the onset of diabetes, as well as other common metabolic disorders including hypertension, heart disease, vision impairment, and renal failure. Nowadays, diabetes mellitus has emerged as one of the greatest threats to public health [281,282]. Hence, the early detection of glucose is of paramount significance.

A novel nanosensor has been developed for glucose sensing, using boric acid-modified sulfur and nitrogen co-doped GQDs ((B)/S,N-GQDs). Boric acid was selected for its easy availability and the feasibility of one-step surface modification of S,N-GQDs, with boric acid groups serving as recognition sites for glucose (Figure 14). The interaction between the cis-diol units of glucose and the boric acid groups on the surface of S,N-GQDs forms rigid (B)/S,N-GQDs-glucose structures, restricting intramolecular movement and resulting in increased photoluminescence intensity. The fluorescence response was utilized for glucose quantification, achieving a LOD of 5.5 µM (Figure 14a) [283]. In a separate investigation, boron- and sulfur-doped CDs (B,S-CDs) were synthesized from 3-thiophenylboronic acid for glucose sensing in saliva due to its compatibility with the CD core. After functionalizing sulfur-doped CDs with boronic acid, new sites selective for glucose, through interaction with the glucose cis-diol groups, were created (Figure 14b). The fluorescence intensity was used to measure glucose concentrations from 1 to 250 µM, with a LOD of 0.57 mM [284].

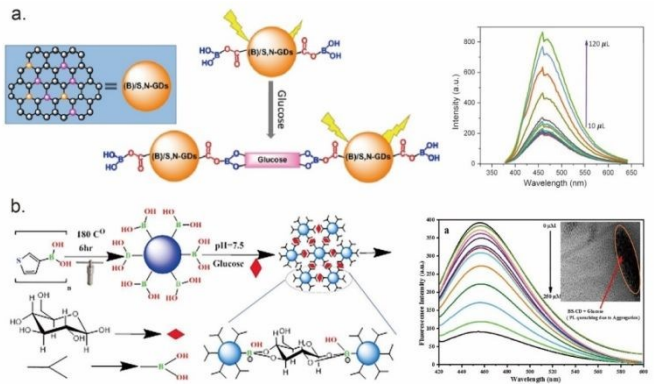

Figure 14. (a) Mechanism of (B)/S,N-GQDs nanosensor and the fluorescence intensity change with different volumes (10–120 µL) of glucose solution (5.5 mM). Reproduced from ref. 283 with permission from Elsevier B.V., copyright© 2020. (b) Synthesis and principle for the application of B,S-CDs to glucose sensing. Reproduced from ref. 284 with permission from Elsevier B.V., copyright© 2021.

8.2 Dopamine (DA) Determination

Dopamine, 3,4-dihydroxyphenethylamine (DA), is a neurotransmitter derived from catecholamine, and plays critical

View Article Online
DOI: 10.1039/D6TB00190D

roles in the functioning of renal, cardiovascular, and central nervous systems, etc. in the body [285]. In the human brain, the concentration of endogenous dopamine is typically 0.01−1 mM [286,287]. Deficiencies in dopamine levels primarily contribute to neurological disorders, which can be manifested as neurological diseases such as dementia, Parkinson's disease, schizophrenia, epilepsy, depression, and attention deficit hyperactivity disorder [288]. Therefore, the selective and sensitive detection of dopamine is crucial for the diagnosis and monitoring of these conditions.

Highly sensitive nitrogen- and boron-doped CDs were synthesized from melamine and 3-carboxyphenylboronic acid by a hydrothermal method. The resulting blue-fluorescent MPBCDs, stabilized by magnetic stirring with β-cyclodextrin (β-CD), showed excitation-dependent emission, along with biocompatibility and non-toxicity. Furthermore, a β-MPB-CDs-PYL probe, obtained by the addition of pyridoxal (PYL), gave enhanced fluorescence towards DA [289] (Figure 15a). Nitrogen-doped GQDs modified with β-cyclodextrin and vitamin B6 cofactor were prepared for the selective sensing of dopamine in human serum using a 'turn-on' fluorometric method (Figure 15b) [290]. Kumar et al. synthesized nitrogen-doped CDs (N-CDs) for dopamine detection, cell imaging, and fluorescent ink applications [291]. Boron and nitrogen co-doped silicon-CDs (B,N-Si-CDs) were for dopamine sensing by colorimetry and fluorimetry [292]. Phthalocyanine-nitrogen-doped GQD conjugates were developed for the detection of dopamine by electrochemical processes [293].

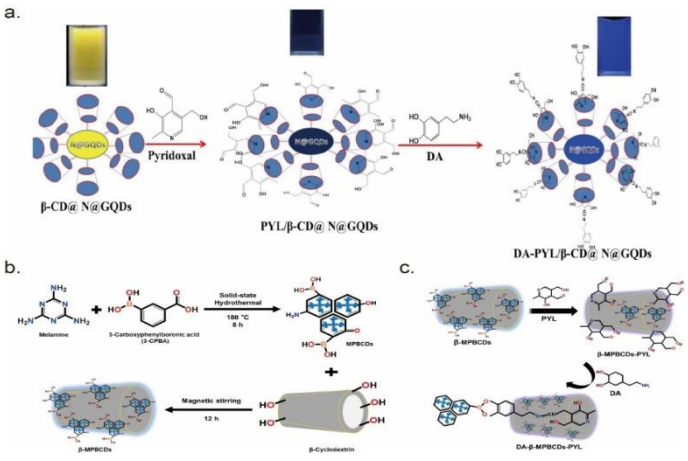

Figure 15. (a) Sensing of DA via PYL/β-CD/N@GQDs with corresponding color changes. Reproduced from ref. 289 with permission from Elsevier Ltd, copyright© 2023. (b) Synthesis of MPBCDs and their stabilization by β-cyclodextrin (β-MPBCDs) and (c) Plausible mechanism for the fluorescent turn-on detection of DA using β-MPBCDs-PYL probe. Reproduced from ref. 290 with permission from Elsevier B.V., copyright© 2020.

8.3 Ascorbic Acid (AA) Determination

The assay of ascorbic acid (AA) and uric acid (UA) holds significant importance in biomedical sciences due to their crucial roles in various human metabolic processes [294,295]. AA, also known as vitamin C, is a water-soluble vitamin found in many foods and dietary supplements. Within the body, it functions as a potent natural antioxidant, scavenging free radicals to safeguard cells from damage. However, excessive intake can result in adverse effects such as diarrhea, taste alteration, kidney stones, and other symptoms [296]. It is believed to aid in the prevention and treatment of conditions such as colds, mental disorders, infertility, cancer, and certain HIV-related clinical symptoms [297–299].

To assay AA, Yang et al. developed a ratiometric fluorescence sensor using ZnCdS QDs embedded in a molecularly imprinted polymer (ZnCdS QDs@MIP) and silica-coated CdTeS QDs (CdTeS QDs@SiO2) (Figure 16a) [297]. This sensor exhibited a linear fluorescence quenching response to AA in the 1–500 μM range, with a LOD of 0.78 μM. Nitrogen and copper co-doped CDs (Cu,N-CDs) were synthesized by the solvothermal carbonization of folic acid and $CuCl_2$. The Cu,N-CDs showed a linear fluorescence quenching response to AA in the 0.02–40 μM range, with a LOD of 17.8 nM [300]. Zhu et al. synthesized V_2O_5 nanobelts which can quench the fluorescence of nitrogen-doped CDs (N-CDs) through the IFE. In the presence of AA, the fluorescence of N-CDs can be restored via a redox reaction with the V_2O_5 nanobelts. Furthermore, in the presence of both alkaline phosphatase (ALP) and ascorbyl-2-phosphate (AAP), the fluorescence of N-CDs can also be restored, as AAP undergoes hydrolysis to AA by ALP (Figure 16b) [301]. An 'on-off-on' fluorescent sensor was developed using sulfur and nitrogen co-doped CDs (S,N-CDs) for the detection of both Cr^{6+} and AA, with excellent selectivity and anti-interference capabilities against over 30 interfering substances. In liquid-phase detection, the sensor had a linear detection range of 1–1000 μM and a LOD of 0.28 μM for AA. For solid-phase detection, S,N-CDs were embedded into polyvinyl alcohol to give a visual fluorescent film sensor which, when irradiated at 365 nm, allowed easy and accurate on-site assay of Cr^{6+} and AA. The

linear detection ranges were 0.1–50 μM and 10–500 μM, respectively, with LODs of 92.5 nM and 7.0 μM, respectively [302].

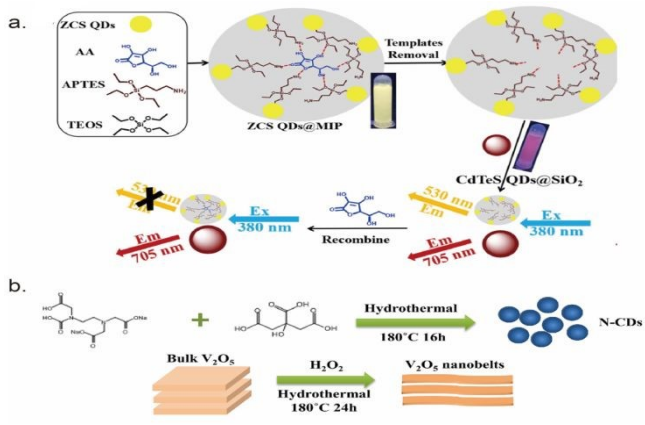

Figure 16. (a) Schematic illustrations of ZnCdS QDs@MIP/CdTeS QDs@SiO_2 sensor for the recognition of AA. Reproduced from ref. 297 with permission from Elsevier B.V., copyright© 2021. (b) Preparation of N-CDs and V_2O_5 nanobelts. Reproduced from ref. 301 with permission from Elsevier B.V., copyright© 2019.

8.4 Glutathione (GSH) determination

Glutathione (GSH), a thiol-containing tripeptide, is essential in biological systems, contributing to immune function maintenance and cellular redox balance. It safeguards against oxidative stress caused by free radicals and ROS, regulating intracellular redox equilibrium. The typical concentration of GSH in animal cells ranges from 0.5 to 10 mM, while in physiological fluids it varies from 2 to 12 μM [303]. Consequently, GSH serves as a crucial biomarker for human health, with abnormal levels associated with various diseases, including cancer, neurodegenerative disorders, impaired growth, liver damage, and cardiovascular ailments [304]. By a solvothermal method in DMF, Liao et al. prepared multicolor N-CDs from naphthalenetetracarboxylic dianhydride, with different alkylamines as passivators. Yellow-emitting CDs were uniformly dispersed (average diameter about 2.4 nm), and could be used to assay GSH in the 1–70 μM range with a LOD of 0.07 mM [305].

Conclusions and future perspectives

This paper reviews the synthesis, properties, modulation, and applications of the fluorescence properties of CDs to the analysis of heavy metals and some molecules of biological interest. The possible use of CD composites for treating polluted water by the extraction of heavy metals is discussed. CDs show great promise for detecting and removing heavy metals due to their unique optical properties, stability, low toxicity, and biocompatibility. Their size, shape, and surface features can be tailored by different synthesis methods to enhance performance in environmental and biomedical applications. However, despite these advantages, CDs still face certain challenges and limitations. Firstly, while there is a diversity of synthesis methods, they still need to be optimized to achieve higher yields, better reproducibility, and lower costs. Secondly, the long-term stability and ecological impacts of CDs in real-world environments are not yet fully understood, and further studies are required to assess their potential dangers. Future research should also explore new functionalization strategies to enhance the selectivity and sensitivity of CDs for specific pollutants. With advancements in nanotechnology and materials science, it is expected that novel CD composites will be developed, expanding their applications in environmental remediation, energy conversion, and biomedicine. Strengthening industry collaboration to transition CDs from the laboratory to practical applications is a key direction for future development.

Author contributions

D.D.S. and Y.X. drafted the manuscript; M.H. and A.K.D.D reviewed and edited the manuscript. All authors have read and agreed to the submitted version of the manuscript.

Conflicts of interest

There are no conflicts to declare.

Data availability

Data sharing is not applicable to this article as no new data were created or analysed in this review.

Acknowledgements

The authors gratefully acknowledge Dr. John S. Lomas for his invaluable supervision, guidance, and support throughout this work. His passing is a great loss, and his memory will be deeply respected. The authors thank the China Scholarship Council for a research grant (for Y.X.) and the Ministry of Higher Education,

Research and Innovation, Senegal, for a mobility grant (for D.D.S.). The ANR (Agence Nationale de la Recherche) and the CGI (Commissariat à l'Investissement d'Avenir) are thanked for financial support through IdEx and Labex SEAM (Science and Engineering for Advanced Materials and devices): ANR-18-IDEX-0001(MANO4T Emergence project), ANR 10 LABX 0096 and ANR 11 IDEX 05 02.

Notes and references

1 L. Liang, Z. Wang and J. Li, *Journal of Cleaner Production*, 2019, **237**, 117649.
2 N. Akhtar, M. I. Syakir Ishak, S. A. Bhawani and K. Umar, *Water*, 2021, **13**, 2660.
3 T. Sato, M. Qadir, S. Yamamoto, T. Endo and A. Zahoor, *Agricultural Water Management*, 2013, **130**, 1–13.
4 S. Sahu, R. Roy and R. Anand, *ACS Sens.*, 2022, **7**, 704–715.
5 T. Bhattacharjee, A. Konwar, J. S. Boruah, D. Chowdhury and G. Majumdar, *Journal of Hazardous Materials Advances*, 2023, **10**, 100295.
6 I. Kaur, V. Batra, N. Kumar Reddy Bogireddy, S. D. Torres Landa and V. Agarwal, *Food Chemistry*, 2023, **406**, 135029.
7 J. Mei, Z. Qiu, T. Gao, Q. Wu, F. Zheng, J. Jiang, K. Liu, Y. Huang, H. Wang and Q. Li, *Langmuir*, 2023, **39**, 4413–4426.
8 S. Kapoor, A. Jha, H. Ahmad and S. S. Islam, *ACS Omega*, 2020, **5**, 18831–18841.
9 S. A. I. Sheikh Mohd Ghazali, I. Fatimah, Z. N. Zamil, N. N. Zulkifli and N. Adam, *Open Chemistry*, 2023, **21**, 20220285.
10 M. Nazar, M. Hasan, B. Wirjosentono, B. A. Gani and C. E. Nada, *ACS Omega*, 2024, **9**, 20571–20581.
11 R. B. González-González, L. T. González, M. Madou, C. Leyva-Porras, S. O. Martinez-Chapa and A. Mendoza, *Nanomaterials*, 2022, **12**, 298.
12 P. Saheeda, K. Sabira, J. Joseph and S. Jayaleksmi, *Materials Chemistry and Physics*, 2019, **225**, 8–15.
13 K. Ganesan, C. Hayagreevan, A. J. Jeevagan, T. Adinaveen, P. L. Sophie, M. Amalraj and D. S. Bhuvaneshwari, *J Appl Electrochem*, 2024, **54**, 89–102.
14 J. Xu, Q. Liang, Z. Li, V. Yu. Osipov, Y. Lin, B. Ge, Q. Xu, J. Zhu and H. Bi, *Advanced Materials*, 2022, **34**, 2200011.
15 A. V.A, S. P, R. Poovathinthodiyil and R. N.K, *Materials Research Bulletin*, 2021, **139**, 111284.
16 Y. Zhang, S. Zhang, B. Tan, L. Guo and H. Li, *Journal of Colloid and Interface Science*, 2021, **604**, 1–14.
17 Y. Xu, Z. Xu, C. Chen, W. Ye, B. Guo, J. Qiu, J. Zhuang, C. Hu, B. Lei, G. Hu and Y. Liu, *Dyes and Pigments*, 2023, **214**, 111204.
18 H. Qi, L. Qiu, X. Zhang, T. Yi, J. Jing, R. Sami, S. F. Alanazi, Z. Alqahtani, M. D. Aljabri and M. M. Rahman, *RSC Adv.*, 2023, **13**, 2663–2671.
19 H. Saljoughi, F. Khakbaz and M. Mahani, *Photodiagnosis and Photodynamic Therapy*, 2020, **30**, 101687.
20 T. Li, D. Zhao, L. Li, Y. Meng, Y. Xie, D. Feng, F. Wu, D. Xie, Y. Liu and Y. Mei, *Bioresource Technology*, 2024, **394**, 130268.
21 Y. Duan, J. Tan, Z. Huang, Q. Deng, S. Liu, G. Wang, L. Li and L. Zhou, *Carbohydrate Polymers*, 2020, **249**, 116882.
22 S. Zhao, K. Yang, L. Jiang, J. Xiao, B. Wang, L. Zeng, X. Song and M. Lan, *ACS Appl. Nano Mater.*, 2021, **4**, 10528–10533.
23 Q. Wu, L. Wang, Y. Yan, S. Li, S. Yu, J. Wang and L. Huang, *ACS Sustainable Chem. Eng.*, 2022, **10**, 3027–3036.
24 P. K. Pandey, Preeti, K. Rawat, T. Prasad and H. B. Bohidar, *J. Mater. Chem. B*, 2020, **8**, 1277–1289.
25 K. K. Gudimella, G. Gedda, P. S. Kumar, B. K. Babu, B. Yamajala, B. V. Rao, P. P. Singh, D. Kumar and A. Sharma, *Environmental Research*, 2022, **204**, 111854.
26 X. Yang, D. Wang, N. Luo, M. Feng, X. Peng and X. Liao, *Spectrochimica Acta Part A: Molecular and Biomolecular Spectroscopy*, 2020, **239**, 118462.
27 D. Sun, T. Liu, C. Wang, L. Yang, S. Yang and K. Zhuo, *Spectrochimica Acta Part A: Molecular and Biomolecular Spectroscopy*, 2020, **240**, 118598.
28 S. Patra, M. Singh, S. Subudhi, M. Mandal, A. K. Nayak, B. B. Sahu and P. Mahanandia, *Journal of Photochemistry and Photobiology A: Chemistry*, 2023, **442**, 114779.
29 A. Sharma and J. Das, *J Nanobiotechnol*, 2019, **17**, 92.
30 Y. D. Yat, H. C. Y. Foo, I. S. Tan, M. K. Lam, P. L. Show and B. W. L. Ng, *Journal of Environmental Chemical Engineering*, 2024, **12**, 112715.
31 A. Kim, J. K. Dash, P. Kumar and R. Patel, *ACS Appl. Electron. Mater.*, 2022, **4**, 27–58.
32 D. Rocco, V. G. Moldoveanu, M. Feroci, M. Bortolami and F. Vetica, *ChemElectroChem*, 2023, **10**, e202201104.
33 S. Ahirwar, S. Mallick and D. Bahadur, *ACS Omega*, 2017, **2**, 8343–8353.
34 M. He, X. Guo, J. Huang, H. Shen, Q. Zeng and L. Wang, *Carbon*, 2018, **140**, 508–520.
35 Y. Liu, S. Roy, S. Sarkar, J. Xu, Y. Zhao and J. Zhang, *Carbon Energy*, 2021, **3**, 795–826.
36 D. Reyes, M. Camacho, M. Camacho, M. Mayorga, D. Weathers, G. Salamo, Z. Wang and A. Neogi, *Nanoscale Res Lett*, 2016, **11**, 424.
37 F. R. U. Cortes, E. Falomir, C. Doñate-Buendía and G. Mínguez-Vega, *J. Phys. Chem. C*, 2025, **129**, 10378–10414.
38 S. Kang, H. Han, K. Lee and K. M. Kim, *ACS Omega*, 2022, **7**, 2074–2081.
39 D. Ozyurt, M. A. Kobaisi, R. K. Hocking and B. Fox, *Carbon Trends*, 2023, **12**, 100276.
40 T. R. DeMeester and L. F. Johnson, *Am J Surg*, 1975, **129**, 94–100.
41 H. Huang, Y. Cui, M. Liu, J. Chen, Q. Wan, Y. Wen, F. Deng, N. Zhou, X. Zhang and Y. Wei, *Journal of Colloid and Interface Science*, 2018, **532**, 767–773.
42 S. Y. Park, H. U. Lee, E. S. Park, S. C. Lee, J.-W. Lee, S. W. Jeong, C. H. Kim, Y.-C. Lee, Y. S. Huh and J. Lee, *ACS Appl. Mater. Interfaces*, 2014, **6**, 3365–3370.
43 K. P, A. R. Cherian, U. Sirimahachai, D. A. Thadathil, A. Varghese and G. Hegde, *Journal of Environmental Chemical Engineering*, 2022, **10**, 107209.
44 Y.-L. T. Ngo, P. L. Nguyen, J. Jana, W. M. Choi, J. S. Chung and S. H. Hur, *Analytica Chimica Acta*, 2021, **1147**, 187–198.
45 S. M. Pirot, K. M. Omer, A. H. Alshatteri, G. K. Ali and O. B. A. Shatery, *Spectrochimica Acta Part A: Molecular and Biomolecular Spectroscopy*, 2023, **291**, 122340.
46 Q. Tan, X. An, S. Pan, S. Zhen, Y. Hu and X. Hu, *Optical Materials*, 2022, **123**, 111830.
47 A. Visheratina, L. Hesami, A. K. Wilson, N. Baalbaki, N. Noginova, M. A. Noginov and N. A. Kotov, *Chirality*, 2022, **34**, 1503–1514.
48 Y. S. Alqahtani, A. M. Mahmoud and M. M. El-Wekil, *Talanta*, 2023, **253**, 124024.
49 H. Zhou, Y. Ren, Z. Li, W. He and Z. Li, *Coatings*, 2022, **12**, 1042.

50 H. Sun, S. Xu, Z. Chen, F. Liu, S. Zong, Z. Wang and C. Wang, *Materials Research Bulletin*, 2023, **159**, 112092.
51 G. Ma, R. Wang, M. Zhang, Z. Dong, A. Zhang, M. Qu, L. Gao, Y. Wei and J. Wei, *Spectrochimica Acta Part A: Molecular and Biomolecular Spectroscopy*, 2023, **289**, 122178.
52 Y. Hao, L. Yu, T. Li, L. Chen, X. Han and F. Chai, *Spectrochimica Acta Part A: Molecular and Biomolecular Spectroscopy*, 2023, **285**, 121865.
53 K. Tungare, M. Bhori, K. S. Racherla and S. Sawant, *3 Biotech*, 2020, **10**, 540.
54 H. B. A. Sousa, C. S. M. Martins and J. A. V. Prior, *Nanomaterials*, 2021, **11**, 611.
55 X. Zhai, P. Zhang, C. Liu, T. Bai, W. Li, L. Dai and W. Liu, *Chem. Commun.*, 2012, **48**, 7955.
56 C. Zhang, Y. Cui, L. Song, X. Liu and Z. Hu, *Talanta*, 2016, **150**, 54–60.
57 M. B. Gawande, S. N. Shelke, R. Zboril and R. S. Varma, *Acc. Chem. Res.*, 2014, **47**, 1338–1348.
58 S. Nizamuddin, H. A. Baloch, M. T. H. Siddiqui, N. M. Mubarak, M. M. Tunio, A. W. Bhutto, A. S. Jatoi, G. J. Griffin and M. P. Srinivasan, *Rev Environ Sci Biotechnol*, 2018, **17**, 813–837.
59 M. B. Schütz, L. Xiao, T. Lehnen, T. Fischer and S. Mathur, *International Materials Reviews*, 2018, **63**, 341–374.
60 L. Carassiti, A. Jones, P. Harrison, P. S. Dobson, S. Kingman, I. MacLaren and D. H. Gregory, *Energy Environ. Sci.*, 2011, **4**, 1503.
61 S. Yadav, A. Kumar and D. Kumar, *Materials Science for Energy Technologies*, 2023, **6**, 260–266.
62 S. Vibhuti Atulbhai, B. Swapna and S. Kumar Kailasa, *Spectrochimica Acta Part A: Molecular and Biomolecular Spectroscopy*, 2023, **287**, 122098.
63 M. Ahmed Abdel Hamid, S. H. Elagamy, A. Gamal and F. R. Mansour, *Spectrochimica Acta Part A: Molecular and Biomolecular Spectroscopy*, 2023, **293**, 122440.
64 R. Wang, K.-Q. Lu, Z.-R. Tang and Y.-J. Xu, *J. Mater. Chem. A*, 2017, **5**, 3717–3734.
65 L. Zhu, Y. Yin, C.-F. Wang and S. Chen, *J. Mater. Chem. C*, 2013, **1**, 4925.
66 C. Kang, Y. Huang, H. Yang, X. F. Yan and Z. P. Chen, *Nanomaterials*, 2020, **10**, 2316.
67 C. Tan, C. Zhou, X. Peng, H. Zhi, D. Wang, Q. Zhan and S. He, *Nanoscale Res Lett*, 2018, **13**, 272.
68 C.-B. Ma, Z.-T. Zhu, H.-X. Wang, X. Huang, X. Zhang, X. Qi, H.-L. Zhang, Y. Zhu, X. Deng, Y. Peng, Y. Han and H. Zhang, *Nanoscale*, 2015, **7**, 10162–10169.
69 B. Chen, F. Li, S. Li, W. Weng, H. Guo, T. Guo, X. Zhang, Y. Chen, T. Huang, X. Hong, S. You, Y. Lin, K. Zeng and S. Chen, *Nanoscale*, 2013, **5**, 1967.
70 Z. Zhu, R. Li, Y. Li, P. Pan, J. Liu, Y. Qi, B. Zhou and Z. Yang, *Materials Chemistry and Physics*, 2023, **296**, 127300.
71 Y. Li, J. Chen, Y. Wang, H. Li, J. Yin, M. Li, L. Wang, H. Sun and L. Chen, *Applied Surface Science*, 2021, **538**, 148151.
72 N. A. S. Omar, Y. W. Fen, R. Irmawati, H. S. Hashim, N. S. M. Ramdzan and N. I. M. Fauzi, *Nanomaterials*, 2022, **12**, 2365.
73 J. Hou, J. Yan, Q. Zhao, Y. Li, H. Ding and L. Ding, *Nanoscale*, 2013, **5**, 9558.
74 R. De Boëver, J. R. Town, X. Li and J. P. Claverie, *Chemistry A European J*, 2022, **28**, e202200748.
75 J. Ren, H. Opoku, S. Tang, L. Edman and J. Wang, *Advanced Science*, 2024, **11**, 2405472.
76 H. Liu, X. Zhong, Q. Pan, Y. Zhang, W. Deng, G. Zou, H. Hou and X. Ji, *Coordination Chemistry Reviews*, 2024, **498**, 215468.
77 Y. Hu, O. Seivert, Y. Tang, H. E. Karahan and A. Bianco, *Angew Chem Int Ed*, 2024, **63**, e202412341.
78 N. Ullal, R. Mehta and D. Sunil, *Analyst*, 2024, **149**, 1680–1700.
79 J. B. Essner, J. A. Kist, L. Polo-Parada and G. A. Baker, *Chem. Mater.*, 2018, **30**, 1878–1887.
80 M. Pan, X. Xie, K. Liu, J. Yang, L. Hong and S. Wang, *Nanomaterials*, 2020, **10**, 930.
81 G. Ge, L. Li, D. Wang, M. Chen, Z. Zeng, W. Xiong, X. Wu and C. Guo, *J. Mater. Chem. B*, 2021, **9**, 6553–6575.
82 N. Shorgar, I. Bhati and P. Jhalora, in *Quantum Dots*, Elsevier, 2023, pp. 53–75.
83 R. Kaimal, V. Vinoth, A. Shrikrishna Salunke, H. Valdés, R. Viswanathan Mangalaraja, B. Aljafari and S. Anandan, *Ultrasonics Sonochemistry*, 2022, **82**, 105868.
84 Z. Feng, K. H. Adolfsson, Y. Xu, H. Fang, M. Hakkarainen and M. Wu, *Sustainable Materials and Technologies*, 2021, **29**, e00304.
85 Y. Lou, X. Hao, L. Liao, K. Zhang, S. Chen, Z. Li, J. Ou, A. Qin and Z. Li, *Nano Select*, 2021, **2**, 1117–1145.
86 P. R. Kharangarh, N. M. Ravindra, G. Singh and S. Umapathy, *Energy Storage*, 2023, **5**, e390.
87 Y. Huo, S. Xiu, L.-Y. Meng and B. Quan, *Chemical Engineering Journal*, 2023, **451**, 138572.
88 T. V. De Medeiros, J. Manioudakis, F. Noun, J.-R. Macairan, F. Victoria and R. Naccache, *J. Mater. Chem. C*, 2019, **7**, 7175–7195.
89 X. Zhang, C. Wei, Y. Li and D. Yu, *TrAC Trends in Analytical Chemistry*, 2019, **116**, 109–121.
90 P. Singh, V. Bhankar, S. Kumar and K. Kumar, *Advances in Colloid and Interface Science*, 2024, **328**, 103182.
91 L. Tian, D. Ghosh, W. Chen, S. Pradhan, X. Chang and S. Chen, *Chem. Mater.*, 2009, **21**, 2803–2809.
92 S. N. Baker and G. A. Baker, *Angew Chem Int Ed*, 2010, **49**, 6726–6744.
93 A. Hemmati, H. Emadi and S. R. Nabavi, *ACS Omega*, 2023, **8**, 20987–20999.
94 Y. Dong, J. Lin, Y. Chen, F. Fu, Y. Chi and G. Chen, *Nanoscale*, 2014, **6**, 7410–7415.
95 S. C. Ray, A. Saha, N. R. Jana and R. Sarkar, *J. Phys. Chem. C*, 2009, **113**, 18546–18551.
96 S.-L. Hu, K.-Y. Niu, J. Sun, J. Yang, N.-Q. Zhao and X.-W. Du, *J. Mater. Chem.*, 2009, **19**, 484–488.
97 P. Miao, K. Han, Y. Tang, B. Wang, T. Lin and W. Cheng, *Nanoscale*, 2015, **7**, 1586–1595.
98 S. Zhu, Y. Song, X. Zhao, J. Shao, J. Zhang and B. Yang, *Nano Res.*, 2015, **8**, 355–381.
99 S. Qu, X. Liu, X. Guo, M. Chu, L. Zhang and D. Shen, *Adv Funct Materials*, 2014, **24**, 2689–2695.
100 D. Li, D. Han, S.-N. Qu, L. Liu, P.-T. Jing, D. Zhou, W.-Y. Ji, X.-Y. Wang, T.-F. Zhang and D.-Z. Shen, *Light Sci Appl*, 2016, **5**, e16120–e16120.
101 H. Shi, Y. Wang, X. Huang, P. Liang, Y. Tang, Y. Zhang, N. Fu, W. Huang and X. Dong, *J. Mater. Chem. B*, 2018, **6**, 7402–7410.
102 B. Wang and S. Lu, *Matter*, 2022, **5**, 110–149.
103 W. R. Algar, M. Massey, K. Rees, R. Higgins, K. D. Krause, G. H. Darwish, W. J. Peveler, Z. Xiao, H.-Y. Tsai, R. Gupta, K. Lix, M. V. Tran and H. Kim, *Chem. Rev.*, 2021, **121**, 9243–9358.
104 X. Wang, K. Qu, B. Xu, J. Ren and X. Qu, *Nano Res.*, 2011, **4**, 908–920.
105 B. Van Dam, H. Nie, B. Ju, E. Marino, J. M. J. Paulusse, P. Schall, M. Li and K. Dohnalová, *Small*, 2017, **13**, 1702098.
106 Z.-A. Qiao, Y. Wang, Y. Gao, H. Li, T. Dai, Y. Liu and Q. Huo, *Chem. Commun.*, 2010, **46**, 8812.

107 H. Li, X. He, Z. Kang, H. Huang, Y. Liu, J. Liu, S. Lian, C. H. A. Tsang, X. Yang and S. Lee, *Angewandte Chemie*, 2010, **122**, 4532–4536.
108 J. Valenta, *Nanoscience Methods*, 2014, **3**, 11–27.
109 Y.-P. Sun, B. Zhou, Y. Lin, W. Wang, K. A. S. Fernando, P. Pathak, M. J. Meziani, B. A. Harruff, X. Wang, H. Wang, P. G. Luo, H. Yang, M. E. Kose, B. Chen, L. M. Veca and S.-Y. Xie, *J. Am. Chem. Soc.*, 2006, **128**, 7756–7757.
110 J. Liu, Y. Geng, D. Li, H. Yao, Z. Huo, Y. Li, K. Zhang, S. Zhu, H. Wei, W. Xu, J. Jiang and B. Yang, *Advanced Materials*, 2021, **33**, 2007162.
111 S. Zhu, J. Zhang, C. Qiao, S. Tang, Y. Li, W. Yuan, B. Li, L. Tian, F. Liu, R. Hu, H. Gao, H. Wei, H. Zhang, H. Sun and B. Yang, *Chem. Commun.*, 2011, **47**, 6858.
112 Y. Liu, Y. Liu, S.-J. Park, Y. Zhang, T. Kim, S. Chae, M. Park and H.-Y. Kim, *J. Mater. Chem. A*, 2015, **3**, 17747–17754.
113 W. Kong, H. Wu, Z. Ye, R. Li, T. Xu and B. Zhang, *Journal of Luminescence*, 2014, **148**, 238–242.
114 J. Ren, F. Weber, F. Weigert, Y. Wang, S. Choudhury, J. Xiao, I. Lauermann, U. Resch-Genger, A. Bande and T. Petit, *Nanoscale*, 2019, **11**, 2056–2064.
115 L. Cao, X. Wang, M. J. Meziani, F. Lu, H. Wang, P. G. Luo, Y. Lin, B. A. Harruff, L. M. Veca, D. Murray, S.-Y. Xie and Y.-P. Sun, *J. Am. Chem. Soc.*, 2007, **129**, 11318–11319.
116 J. Shen, Y. Zhu, C. Chen, X. Yang and C. Li, *Chem. Commun.*, 2011, **47**, 2580–2582.
117 X. Wen, P. Yu, Y.-R. Toh, X. Ma and J. Tang, *Chem. Commun.*, 2014, **50**, 4703–4706.
118 J. Zong, Y. Zhu, X. Yang, J. Shen and C. Li, *Chem. Commun.*, 2011, **47**, 764–766.
119 D. Li, E. V. Ushakova, A. L. Rogach and S. Qu, *Small*, 2021, **17**, 2102325.
120 L. Li, X. Ren, P. Bai, Y. Liu, W. Xu, J. Xie and R. Zhang, *New Carbon Materials*, 2021, **36**, 632–638.
121 S. Lu, L. Sui, J. Liu, S. Zhu, A. Chen, M. Jin and B. Yang, *Advanced Materials*, 2017, **29**, 1603443.
122 Y. Cui, Z. Hu, C. Zhang and X. Liu, *J. Mater. Chem. B*, 2014, **2**, 6947–6952.
123 Q. Liu, B. Guo, Z. Rao, B. Zhang and J. R. Gong, *Nano Lett.*, 2013, **13**, 2436–2441.
124 B. Yin, J. Deng, X. Peng, Q. Long, J. Zhao, Q. Lu, Q. Chen, H. Li, H. Tang, Y. Zhang and S. Yao, *Analyst*, 2013, **138**, 6551.
125 D. Tang, H. Zhang, H. Huang, R. Liu, Y. Han, Y. Liu, C. Tong and Z. Kang, *Dalton Trans.*, 2013, **42**, 6285.
126 H. Zhang, H. Ming, S. Lian, H. Huang, H. Li, L. Zhang, Y. Liu, Z. Kang and S.-T. Lee, *Dalton Trans.*, 2011, **40**, 10822.
127 Y. Song, S. Zhu and B. Yang, *RSC Adv.*, 2014, **4**, 27184.
128 P. G. Luo, S. Sahu, S.-T. Yang, S. K. Sonkar, J. Wang, H. Wang, G. E. LeCroy, L. Cao and Y.-P. Sun, *J. Mater. Chem. B*, 2013, **1**, 2116.
129 Y.-Y. Liu, N.-Y. Yu, W.-D. Fang, Q.-G. Tan, R. Ji, L.-Y. Yang, S. Wei, X.-W. Zhang and A.-J. Miao, *Nat Commun*, 2021, **12**, 812.
130 H. Tao, K. Yang, Z. Ma, J. Wan, Y. Zhang, Z. Kang and Z. Liu, *Small*, 2012, **8**, 281–290.
131 X. Zhai, P. Zhang, C. Liu, T. Bai, W. Li, L. Dai and W. Liu, *Chem. Commun.*, 2012, **48**, 7955.
132 J. Deng, Q. Lu, N. Mi, H. Li, M. Liu, M. Xu, L. Tan, Q. Xie, Y. Zhang and S. Yao, *Chemistry A European J*, 2014, **20**, 4993–4999.
133 K. Jiang, S. Sun, L. Zhang, Y. Wang, C. Cai and H. Lin, *ACS Appl. Mater. Interfaces*, 2015, **7**, 23231–23238.
134 B. Kong, A. Zhu, C. Ding, X. Zhao, B. Li and Y. Tian, *Advanced Materials*, 2012, **24**, 5844–5848.
135 E. J. Goh, K. S. Kim, Y. R. Kim, H. S. Jung, S. Beack, W. H. Kong, G. Scarcelli, S. H. Yun and S. K. Hahn, *Biomacromolecules*, 2012, **13**, 2554–2561.
136 H. Belkahla, R. Boudjemaa, V. Caorsi, D. Pineau, A. Curcio, J. S. Lomas, P. Decorse, A. Chevillot-Biraud, T. Azaïs, C. Wilhelm, H. Randriamahazaka and M. Hémadi, *Nanoscale Adv.*, 2019, **1**, 2571–2579.
137 W. Pang, P. Jiang, S. Ding, Z. Bao, N. Wang, H. Wang, J. Qu, D. Wang, B. Gu and X. Wei, *Adv Healthcare Materials*, 2020, **9**, 2000607.
138 M. Havrdova, K. Hola, J. Skopalik, K. Tomankova, M. Petr, K. Cepe, K. Polakova, J. Tucek, A. B. Bourlinos and R. Zboril, *Carbon*, 2016, **99**, 238–248.
139 M. Usman, Y. Zaheer, M. R. Younis, R. E. Demirdogen, S. Z. Hussain, Y. Sarwar, M. Rehman, W. S. Khan and A. Ihsan, *Colloid and Interface Science Communications*, 2020, **35**, 100243.
140 T. Bhattacharya, S. Preetam, S. Mukherjee, S. Kar, D. S. Roy, H. Singh, A. Ghose, T. Das and G. Mohapatra, *Discover Nano*, 2024, **19**, 122.
141 M. Pan, X. Xie, K. Liu, J. Yang, L. Hong and S. Wang, *Nanomaterials*, 2020, **10**, 930.
142 P. N. Joshi, S. Kundu, S. K. Sanghi and D. Sarkar, in *Smart Drug Delivery System*, ed. A. D. Sezer, InTech, 2016.
143 T. Gao, X. Wang, L.-Y. Yang, H. He, X.-X. Ba, J. Zhao, F.-L. Jiang and Y. Liu, *ACS Appl. Mater. Interfaces*, 2017, **9**, 24846–24856.
144 J. Peng, W. Gao, B. K. Gupta, Z. Liu, R. Romero-Aburto, L. Ge, L. Song, L. B. Alemany, X. Zhan, G. Gao, S. A. Vithayathil, B. A. Kaipparettu, A. A. Marti, T. Hayashi, J.-J. Zhu and P. M. Ajayan, *Nano Lett.*, 2012, **12**, 844–849.
145 M. A. Sk, A. Ananthanarayanan, L. Huang, K. H. Lim and P. Chen, *J. Mater. Chem. C*, 2014, **2**, 6954–6960.
146 F. Yuan, T. Yuan, L. Sui, Z. Wang, Z. Xi, Y. Li, X. Li, L. Fan, Z. Tan, A. Chen, M. Jin and S. Yang, *Nat Commun*, 2018, **9**, 2249.
147 H. Bai, X. Jin, Z. Cheng, H. Zhou, H. Wang, J. Yu, J. Zuo and W. Chen, *Adv Compos Hybrid Mater*, 2023, **6**, 62.
148 R. Liu, D. Wu, S. Liu, K. Koynov, W. Knoll and Q. Li, *Angew Chem Int Ed*, 2009, **48**, 4598–4601.
149 Y. Yang, D. Wu, S. Han, P. Hu and R. Liu, *Chem. Commun.*, 2013, **49**, 4920.
150 B. B. Chen, M. L. Liu, C. M. Li and C. Z. Huang, *Advances in Colloid and Interface Science*, 2019, **270**, 165–190.
151 X. Li, Y. Fu, S. Zhao, J. Xiao, M. Lan, B. Wang, K. Zhang, X. Song and L. Zeng, *Chemical Engineering Journal*, 2022, **430**, 133101.
152 G. Yang, C. Wu, X. Luo, X. Liu, Y. Gao, P. Wu, C. Cai and S. S. Saavedra, *J. Phys. Chem. C*, 2018, **122**, 6483–6492.
153 W. Wei, C. Xu, L. Wu, J. Wang, J. Ren and X. Qu, *Sci Rep*, 2014, **4**, 3564.
154 X. Gong, W. Lu, M. C. Paau, Q. Hu, X. Wu, S. Shuang, C. Dong and M. M. F. Choi, *Analytica Chimica Acta*, 2015, **861**, 74–84.
155 X. Niu, Y. Li, H. Shu and J. Wang, *Nanoscale*, 2016, **8**, 19376–19382.
156 C. Zhang, Z. Hu, L. Song, Y. Cui and X. Liu, *New J. Chem.*, 2015, **39**, 6201–6206.
157 S. Yang, J. Sun, X. Li, W. Zhou, Z. Wang, P. He, G. Ding, X. Xie, Z. Kang and M. Jiang, *J. Mater. Chem. A*, 2014, **2**, 8660.
158 A. B. Bourlinos, G. Trivizas, M. A. Karakassides, M. Baikousi, A. Kouloumpis, D. Gournis, A. Bakandritsos, K. Hola, O. Kozak, R. Zboril, I. Papagiannouli, P. Aloukos and S. Couris, *Carbon*, 2015, **83**, 173–179.
159 C. Zhao, Y. Jiao, Z. Gao, Y. Yang and H. Li, *Journal of Photochemistry and Photobiology A: Chemistry*, 2018, **367**, 137–144.

160 L. Jiang, H. Ding, M. Xu, X. Hu, S. Li, M. Zhang, Q. Zhang, Q. Wang, S. Lu, Y. Tian and H. Bi, *Small*, 2020, **16**, 2000680.
161 F. Wu, H. Su, X. Zhu, K. Wang, Z. Zhang and W.-K. Wong, *J. Mater. Chem. B*, 2016, **4**, 6366–6372.
162 C. Han, H. Xu, R. Wang, K. Wang, Y. Dai, Q. Liu, M. Guo, J. Li and K. Xu, *J. Mater. Chem. B*, 2016, **4**, 5798–5802.
163 X. Chu, G. Ning, Z. Zhou, Y. Liu, Q. Xiao and S. Huang, *Microchim Acta*, 2020, **187**, 659.
164 S. Sun, L. Zhao, D. Wu, H. Zhang, H. Lian, X. Zhao, A. Wu and L. Zeng, *ACS Appl. Bio Mater.*, 2021, **4**, 1969–1975.
165 M. Zhang, T. Zheng, B. Sheng, F. Wu, Q. Zhang, W. Wang, J. Shen, N. Zhou and Y. Sun, *Chemical Engineering Journal*, 2019, **373**, 1054–1063.
166 Q. Jia, J. Ge, W. Liu, X. Zheng, S. Chen, Y. Wen, H. Zhang and P. Wang, *Advanced Materials*, 2018, **30**, 1706090.
167 F. Du, L. Zhang, L. Zhang, M. Zhang, A. Gong, Y. Tan, J. Miao, Y. Gong, M. Sun, H. Ju, C. Wu and S. Zou, *Biomaterials*, 2017, **121**, 109–120.
168 Z. Ji, P. Ai, C. Shao, T. Wang, C. Yan, L. Ye and W. Gu, *ACS Biomater. Sci. Eng.*, 2018, **4**, 2089–2094.
169 T. Luo, Y. Nie, J. Lu, Q. Bi, Z. Cai, X. Song, H. Ai and R. Jin, *Materials & Design*, 2021, **208**, 109878.
170 B. Tian, S. Liu, L. Feng, S. Liu, S. Gai, Y. Dai, L. Xie, B. Liu, P. Yang and Y. Zhao, *Adv Funct Materials*, 2021, **31**, 2100549.
171 W. Wu, L. Zhan, W. Fan, J. Song, X. Li, Z. Li, R. Wang, J. Zhang, J. Zheng, M. Wu and H. Zeng, *Angew Chem Int Ed*, 2015, **54**, 6540–6544.
172 S. Zhu, J. Zhang, X. Liu, B. Li, X. Wang, S. Tang, Q. Meng, Y. Li, C. Shi, R. Hu and B. Yang, *RSC Adv.*, 2012, **2**, 2717.
173 K. P. Loh, Q. Bao, G. Eda and M. Chhowalla, *Nature Chem*, 2010, **2**, 1015–1024.
174 C. Hu, M. Li, J. Qiu and Y.-P. Sun, *Chem. Soc. Rev.*, 2019, **48**, 2315–2337.
175 Z. Qu, X. Zhou, L. Gu, R. Lan, D. Sun, D. Yu and G. Shi, *Chem. Commun.*, 2013, **49**, 9830.
176 H. Chen, Y. Xie, A. M. Kirillov, L. Liu, M. Yu, W. Liu and Y. Tang, *Chem. Commun.*, 2015, **51**, 5036–5039.
177 P. Anilkumar, X. Wang, L. Cao, S. Sahu, J.-H. Liu, P. Wang, K. Korch, K. N. Tackett Ii, A. Parenzan and Y.-P. Sun, *Nanoscale*, 2011, **3**, 2023.
178 H. Zhu, X. Wang, Y. Li, Z. Wang, F. Yang and X. Yang, *Chem. Commun.*, 2009, 5118.
179 Y. Dong, R. Wang, H. Li, J. Shao, Y. Chi, X. Lin and G. Chen, *Carbon*, 2012, **50**, 2810–2815.
180 C. Liu, P. Zhang, F. Tian, W. Li, F. Li and W. Liu, *J. Mater. Chem.*, 2011, **21**, 13163.
181 S. Zhu, Q. Meng, L. Wang, J. Zhang, Y. Song, H. Jin, K. Zhang, H. Sun, H. Wang and B. Yang, *Angew Chem Int Ed*, 2013, **52**, 3953–3957.
182 M. J. Krysmann, A. Kelarakis, P. Dallas and E. P. Giannelis, *J. Am. Chem. Soc.*, 2012, **134**, 747–750.
183 M. Li, C. Hu, C. Yu, S. Wang, P. Zhang and J. Qiu, *Carbon*, 2015, **91**, 291–297.
184 H. Zheng, Q. Wang, Y. Long, H. Zhang, X. Huang and R. Zhu, *Chem. Commun.*, 2011, **47**, 10650.
185 P. Luo, Y. Qiu, X. Guan and L. Jiang, *Phys. Chem. Chem. Phys.*, 2014, **16**, 19011.
186 Y. Dong, R. Dai, T. Dong, Y. Chi and G. Chen, *Nanoscale*, 2014, **6**, 11240–11245.
187 Y. Li, X. Liu, J. Wang, H. Liu, S. Li, Y. Hou, W. Wan, W. Xue, N. Ma and J. Z. Zhang, *J. Phys. Chem. C*, 2016, **120**, 26004–26011.
188 A. S. Helal, M. Hémadi, J. S. Lomas, S. Ammar, A. Abdelhafiz, S. M. El-Sheikh, S. M. Sheta, M. Galanek, M. H. Hassan, J.-K. Chang and J. Li, *Chemical Engineering Journal*, 2025, **507**, 160298.
189 Y. Xiao, A. S. Helal, E. Mazario, A. Mayoral, A. Chevillot-Biraud, P. Decorse, R. Losno, F. Maurel, S. Ammar, J. S. Lomas and M. Hémadi, *Environmental Research*, 2023, **216**, 114569.
190 Y.-C. Lu, J. Chen, A.-J. Wang, N. Bao, J.-J. Feng, W. Wang and L. Shao, *J. Mater. Chem. C*, 2015, **3**, 73–78.
191 X. Lin, M. Xiong, J. Zhang, C. He, X. Ma, H. Zhang, Y. Kuang, M. Yang and Q. Huang, *Microchemical Journal*, 2021, **160**, 105604.
192 F. Zu, F. Yan, Z. Bai, J. Xu, Y. Wang, Y. Huang and X. Zhou, *Microchim Acta*, 2017, **184**, 1899–1914.
193 Y. Guo, L. Zhang, S. Zhang, Y. Yang, X. Chen and M. Zhang, *Biosensors and Bioelectronics*, 2015, **63**, 61–71.
194 L. Zhou, Y. Lin, Z. Huang, J. Ren and X. Qu, *Chem. Commun.*, 2012, **48**, 1147–1149.
195 H. Huang, J.-J. Lv, D.-L. Zhou, N. Bao, Y. Xu, A.-J. Wang and J.-J. Feng, *RSC Adv.*, 2013, **3**, 21691.
196 R. Zhang and W. Chen, *Biosensors and Bioelectronics*, 2014, **55**, 83–90.
197 A. Iqbal, K. Iqbal, L. Xu, B. Li, D. Gong, X. Liu, Y. Guo, W. Liu, W. Qin and H. Guo, *Sensors and Actuators B: Chemical*, 2018, **255**, 1130–1138.
198 X. Hao, S. Dai, J. Wang and Z. Fang, *Luminescence*, 2021, **36**, 721–732.
199 Z. Li, Y. Wang, Y. Ni and S. Kokot, *Sensors and Actuators B: Chemical*, 2015, **207**, 490–497.
200 Y. Hou, Q. Lu, J. Deng, H. Li and Y. Zhang, *Analytica Chimica Acta*, 2015, **866**, 69–74.
201 I. Bremner, *The American Journal of Clinical Nutrition*, 1998, **67**, 1069S-1073S.
202 A. A. Taylor, J. S. Tsuji, M. R. Garry, M. E. McArdle, W. L. Goodfellow, W. J. Adams and C. A. Menzie, *Environmental Management*, 2020, **65**, 131–159.
203 A. Zhu, Z. Luo, C. Ding, B. Li, S. Zhou, R. Wang and Y. Tian, *Analyst*, 2014, **139**, 1945–1952.
204 Y. Pan, M. Xu, L. Cai, L. Qiao, S. Wang, K. Zhang, X. Ran and L. Guo, *ACS Appl. Nano Mater.*, 2024, **7**, 10731–10738.
205 A. Beiraghi and S. A. Najibi-Gehraz, *Sensors and Actuators B: Chemical*, 2017, **253**, 342–351.
206 C. Venkateswara Raju, G. Kalaiyarasan, S. Paramasivam, J. Joseph and S. Senthil Kumar, *Electrochimica Acta*, 2020, **331**, 135391.
207 J. Wang, R. Sheng Li, H. Zhi Zhang, N. Wang, Z. Zhang and C. Z. Huang, *Biosensors and Bioelectronics*, 2017, **97**, 157–163.
208 J. Zong, X. Yang, A. Trinchi, S. Hardin, I. Cole, Y. Zhu, C. Li, T. Muster and G. Wei, *Biosensors and Bioelectronics*, 2014, **51**, 330–335.
209 J. Wang, X. Su, D. Gao, R. Chen, Y. Mu, X. Zhang and L. Wang, *ACS Appl. Nano Mater.*, 2021, **4**, 8990–8997.
210 I. Ibrahim, H. N. Lim, N. M. Huang, Z.-T. Jiang and M. Altarawneh, *Journal of Hazardous Materials*, 2020, **391**, 122248.
211 A. Yiannikourides and G. Latunde-Dada, *Medicines*, 2019, **6**, 85.
212 M. R. Hormozi-Nezhad and M. Taghipour, *Anal. Methods*, 2016, **8**, 4064–4068.
213 J. Yu, N. Song, Y.-K. Zhang, S.-X. Zhong, A.-J. Wang and J. Chen, *Sensors and Actuators B: Chemical*, 2015, **214**, 29–35.
214 Z. Wang, C. Xu, Y. Lu, X. Chen, H. Yuan, G. Wei, G. Ye and J. Chen, *Sensors and Actuators B: Chemical*, 2017, **241**, 1324–1330.
215 C. Li, W. Liu, Y. Ren, X. Sun, W. Pan and J. Wang, *Sensors and Actuators B: Chemical*, 2017, **240**, 941–948.

216 G. Gao, Y.-W. Jiang, H.-R. Jia, J. Yang and F.-G. Wu, *Carbon*, 2018, **134**, 232–243.
217 C. Shen, S. Ge, Y. Pang, F. Xi, J. Liu, X. Dong and P. Chen, *J. Mater. Chem. B*, 2017, **5**, 6593–6600.
218 Y. Vasseghian, F. Almomani and E.-N. Dragoi, *Chemosphere*, 2022, **286**, 131821.
219 E. Mohamed Ali, Y. Zheng, H. Yu and J. Y. Ying, *Anal. Chem.*, 2007, **79**, 9452–9458.
220 Q. Wang, S. Zhang, H. Ge, G. Tian, N. Cao and Y. Li, *Sensors and Actuators B: Chemical*, 2015, **207**, 25–33.
221 A. Kumar, A. R. Chowdhuri, D. Laha, T. K. Mahto, P. Karmakar and S. K. Sahu, *Sensors and Actuators B: Chemical*, 2017, **242**, 679–686.
222 H.-J. Cheng, C.-L. Kao, Y.-F. Chen, P.-C. Huang, C.-Y. Hsu and C.-H. Kuei, *Microchim Acta*, 2017, **184**, 3179–3187.
223 F. Cai, X. Liu, S. Liu, H. Liu and Y. Huang, *RSC Adv.*, 2014, **4**, 52016–52022.
224 R. Vaz, J. Bettini, J. G. F. Júnior, E. D. S. Lima, W. G. Botero, J. C. C. Santos and M. A. Schiavon, *Journal of Photochemistry and Photobiology A: Chemistry*, 2017, **346**, 502–511.
225 Y. Gao, Y. Jiao, W. Lu, Y. Liu, H. Han, X. Gong, M. Xian, S. Shuang and C. Dong, *J. Mater. Chem. B*, 2018, **6**, 6099–6107.
226 S. Wang, H. Niu, S. He and Y. Cai, *RSC Adv.*, 2016, **6**, 107717–107722.
227 P. M. Carrasco, I. García, L. Yate, R. Tena Zaera, G. Cabañero, H. J. Grande and V. Ruiz, *Carbon*, 2016, **109**, 658–665.
228 R. V, S. Misra, M. K. Santra and D. Ottoor, *Journal of Photochemistry and Photobiology A: Chemistry*, 2019, **373**, 28–36.
229 R. Zhang, Y. Zheng, Q. Zhang, Z. Wu, L. Wang, J. Zhang, H. Ren and E. Duan, *Journal of Environmental Chemical Engineering*, 2024, **12**, 112391.
230 Q. Wang, H. Zhang, D. Yu, W. Qin and X. Wu, *Carbon*, 2022, **198**, 162–170.
231 P. Keerthana, A. Kumar Das, M. Bharath, M. Ghosh and A. Varghese, *Journal of Environmental Chemical Engineering*, 2023, **11**, 109325.
232 M. L. Desai, S. Jha, H. Basu, S. Saha, R. K. Singhal and S. K. Kailasa, *Materials Science and Engineering: C*, 2020, **111**, 110778.
233 J. Qiu, D. Zeng, Y. Lin, W. Ye, C. Chen, Z. Xu, G. Hu and Y. Liu, *Spectrochimica Acta Part A: Molecular and Biomolecular Spectroscopy*, 2023, **285**, 121913.
234 P. Krishnaiah, R. Atchudan, S. Perumal, E.-S. Salama, Y. R. Lee and B.-H. Jeon, *Chemosphere*, 2022, **286**, 131764.
235 X. Gao, Y. Zhang, Z. Fu, J. Tian, L. Zhang, W. Li, S. Li and F. Cui, *Optical Materials*, 2023, **143**, 114132.
236 G. Lu, Z. Jia, M. Yu, M. Zhang and C. Xu, *Molecules*, 2023, **28**, 7818.
237 P. Zhu, Z. Zhu, Z. Li, Y. Xu, L. A. Belfiore and J. Tang, *Optical Materials*, 2021, **121**, 111543.
238 S. S. Siwal, H. Kaur, A. K. Saini and V. K. Thakur, *Adv Energy and Sustain Res*, 2022, **3**, 2200062.
239 C. Long, Z. Jiang, J. Shangguan, T. Qing, P. Zhang and B. Feng, *Chemical Engineering Journal*, 2021, **406**, 126848.
240 Y. Qu, X. Xu, R. Huang, W. Qi, R. Su and Z. He, *Chemical Engineering Journal*, 2020, **382**, 123016.
241 G. Sodeifian and R. Behnood, *J Inorg Organomet Polym*, 2020, **30**, 1266–1280.
242 H. Yu, Y. Zhao, C. Zhou, L. Shang, Y. Peng, Y. Cao, L.-Z. Wu, C.-H. Tung and T. Zhang, *J. Mater. Chem. A*, 2014, **2**, 3344.
243 H. Wang, Z. Wei, H. Matsui and S. Zhou, *J. Mater. Chem. A*, 2014, **2**, 15740–15745.
244 C. Sahli, J. Deschamps, L. Royon, J. S. Lomas, R. Briandet and M. Hémadi, *Materials Today Chemistry*, 2024, **35**, 101920.
245 P. Chen, F. Wang, Z.-F. Chen, Q. Zhang, Y. Su, L. Shen, K. Yao, Y. Liu, Z. Cai, W. Lv and G. Liu, *Applied Catalysis B: Environmental*, 2017, **204**, 250–259.
246 S. Sharma, A. Umar, S. K. Mehta, A. O. Ibhadon and S. K. Kansal, *New J. Chem.*, 2018, **42**, 7445–7456.
247 S. Huang, S. Jiang, H. Pang, T. Wen, A. M. Asiri, K. A. Alamry, A. Alsaedi, X. Wang and S. Wang, *Chemical Engineering Journal*, 2019, **368**, 941–950.
248 X. Li, H. Lin, Q. Li, J. Xue, Y. Xu and L. Zhuang, *ACS Appl. Nano Mater.*, 2021, **4**, 3062–3074.
249 L. Wang, C. Cheng, S. Tapas, J. Lei, M. Matsuoka, J. Zhang and F. Zhang, *J. Mater. Chem. A*, 2015, **3**, 13357–13364.
250 L. He, T. Wang, J. An, X. Li, L. Zhang, L. Li, G. Li, X. Wu, Z. Su and C. Wang, *CrystEngComm*, 2014, **16**, 3259.
251 L. Xu, G. Fang, J. Liu, M. Pan, R. Wang and S. Wang, *J. Mater. Chem. A*, 2016, **4**, 15880–15887.
252 G. Li, N. Lv, J. Zhang and J. Ni, *RSC Adv.*, 2017, **7**, 16423–16427.
253 Y. Ma, G. Xu, F. Wei, Y. Cen, Y. Ma, Y. Song, X. Xu, M. Shi, S. Muhammad and Q. Hu, *J. Mater. Chem. C*, 2017, **5**, 8566–8571.
254 X. Guo, Q. Liu, J. Liu, H. Zhang, J. Yu, R. Chen, D. Song, R. Li and J. Wang, *Applied Surface Science*, 2019, **491**, 640–649.
255 Y. Si, X. Li, G. Yang, X. Mie and L. Ge, *J Mater Sci*, 2020, **55**, 13049–13061.
256 X. Qin, T. Qiang, L. Chen and S. Wang, *Microporous and Mesoporous Materials*, 2021, **315**, 110889.
257 Q. Yang, H. Hong and Y. Luo, *Chemical Engineering Journal*, 2020, **392**, 123680.
258 S. Gholizadeh Khasevani, S. Shahsavari and M. R. Gholami, *Materials Research Bulletin*, 2021, **138**, 111204.
259 Y. Zhao, Y. Zhao, G. I. N. Waterhouse, L. Zheng, X. Cao, F. Teng, L. Wu, C. Tung, D. O'Hare and T. Zhang, *Advanced Materials*, 2017, **29**, 1703828.
260 A. L. M. D. De Sousa, W. M. Dos Santos, M. L. De Souza, L. C. P. B. B. Silva, A. E. H. K. Yun, C. S. B. Aguilera, B. D. F. Chagas, L. A. Rolim, R. M. F. Da Silva and P. J. R. Neto, *European Journal of Pharmaceutical Sciences*, 2021, **165**, 105922.
261 W. Yao, X. Wang, Y. Liang, S. Yu, P. Gu, Y. Sun, C. Xu, J. Chen, T. Hayat, A. Alsaedi and X. Wang, *Chemical Engineering Journal*, 2018, **332**, 775–786.
262 H. Asiabi, Y. Yamini, M. Shamsayei, K. Molaei and M. Shamsipur, *Journal of Hazardous Materials*, 2018, **357**, 217–225.
263 M. Zhang, Q. Yao, C. Lu, Z. Li and W. Wang, *ACS Appl. Mater. Interfaces*, 2014, **6**, 20225–20233.
264 K. Iqbal, A. Iqbal, A. M. Kirillov, C. Shan, W. Liu and Y. Tang, *J. Mater. Chem. A*, 2018, **6**, 4515–4524.
265 D. M. Nascimento, Y. L. Nunes, M. C. B. Figueirêdo, H. M. C. De Azeredo, F. A. Aouada, J. P. A. Feitosa, M. F. Rosa and A. Dufresne, *Green Chem.*, 2018, **20**, 2428–2448.
266 Y.-Y. Li, B. Wang, M.-G. Ma and B. Wang, *International Journal of Polymer Science*, 2018, **2018**, 1–18.
267 K. Junka, J. Guo, I. Filpponen, J. Laine and O. J. Rojas, *Biomacromolecules*, 2014, **15**, 876–881.
268 J. Ahn, S. Pak, Y. Song and H. Kim, *Carbohydrate Polymers*, 2021, **255**, 117387.
269 B. Wu, G. Zhu, A. Dufresne and N. Lin, *ACS Appl. Mater. Interfaces*, 2019, **11**, 16048–16058.
270 Y. Guo, J. Bae, Z. Fang, P. Li, F. Zhao and G. Yu, *Chem. Rev.*, 2020, **120**, 7642–7707.

271 M. J. Molaei, *Anal. Methods*, 2020, **12**, 1266–1287.
272 H. Xu, Z. An, H. Zhang, W. Li, X. Yang, Y. Kang, W. Su, M. Zheng and B. Lei, *Materials Research Bulletin*, 2024, **170**, 112590.
273 J. Yang, Z. Luo and M. Wang, *Foods*, 2022, **11**, 1619.
274 X. Zhang, X. Yi, J. Ouyang, S. Wang, D. Xu, X. Qi, P. Jiang, X. Guo and Y. Wu, *Chemical Engineering Journal*, 2024, **479**, 147753.
275 S. Singh and R. Jelinek, *ACS Appl. Polym. Mater.*, 2020, **2**, 2810–2818.
276 Q. Wang, T. Han, C. Miao, W. Qin and X. Wu, *Environ. Sci.: Water Res. Technol.*, 2023, **9**, 2680–2691.
277 X. Qi, J. Peng, X. Zhang, H. Cai, Y. Huang, J. Qiao, Y. Guo, X. Guo and Y. Wu, *Journal of Hazardous Materials*, 2023, **446**, 130689.
278 S. Nayak, S. R. Prasad, D. Mandal and P. Das, *Journal of Hazardous Materials*, 2020, **392**, 122287.
279 M. Barzegarzadeh, M. S. Amini-Fazl and N. Sohrabi, *International Journal of Biological Macromolecules*, 2023, **242**, 124587.
280 W. Liu, H. Jia, J. Zhang, J. Tang, J. Wang and D. Fang, *Microchemical Journal*, 2020, **158**, 105187.
281 C. Dincer, R. Bruch, E. Costa-Rama, M. T. Fernández-Abedul, A. Merkoçi, A. Manz, G. A. Urban and F. Güder, *Advanced Materials*, 2019, **31**, 1806739.
282 M. Govindaraj, A. Srivastava, M. K. Muthukumaran, P.-C. Tsai, Y.-C. Lin, B. K. Raja, J. Rajendran, V. K. Ponnusamy and J. Arockia Selvi, *International Journal of Biological Macromolecules*, 2023, **253**, 126680.
283 M. Masteri-Farahani, F. Ghorbani and N. Mosleh, *Spectrochimica Acta Part A: Molecular and Biomolecular Spectroscopy*, 2021, **245**, 118892.
284 H. O. Othman, R. O. Hassan and A. T. Faizullah, *Microchemical Journal*, 2021, **163**, 105919.
285 E. J. Hird, U. Beierholm, L. De Boer, J. Axelsson, L. Backman and M. Guitart-Masip, *Neurobiology of Aging*, 2022, **118**, 34–43.
286 J. Wang, R. Du, W. Liu, L. Yao, F. Ding, P. Zou, Y. Wang, X. Wang, Q. Zhao and H. Rao, *Sensors and Actuators B: Chemical*, 2019, **290**, 125–132.
287 Y. Ma, A. Y. Chen, X. F. Xie, X. Y. Wang, D. Wang, P. Wang, H. J. Li, J. H. Yang and Y. Li, *Talanta*, 2019, **196**, 563–571.
288 S. Balu, S. Palanisamy, V. Velusamy, T. C. K. Yang and E.-S. I. El-Shafey, *Materials Science and Engineering: C*, 2020, **108**, 110367.
289 R. Sangubotla and J. Kim, *Ceramics International*, 2023, **49**, 16272–16282.
290 A. O. Alqarni, S. A. Alkahtani, A. M. Mahmoud and M. M. El-Wekil, *Spectrochimica Acta Part A: Molecular and Biomolecular Spectroscopy*, 2021, **248**, 119180.
291 A. Kumar, S. Asu, P. Mukherjee, P. Singh, A. Kumari and S. K. Sahu, *Journal of Photochemistry and Photobiology A: Chemistry*, 2021, **406**, 113019.
292 Y.-F. Wang, L. Li, M. Jiang, X. Yang, X. Yu and L. Xu, *Applied Surface Science*, 2022, **573**, 151457.
293 N. Ndebele, P. Sen and T. Nyokong, *Journal of Electroanalytical Chemistry*, 2021, **886**, 115111.
294 M. Ko, L. Mendecki, A. M. Eagleton, C. G. Durbin, R. M. Stolz, Z. Meng and K. A. Mirica, *J. Am. Chem. Soc.*, 2020, **142**, 11717–11733.
295 Z. Fredj, M. Ben Ali, M. N. Abbas and E. Dempsey, *Anal. Methods*, 2020, **12**, 3883–3891.
296 Y. Deng, Y. Zhou, Q. Li and J. Qian, *Anal. Methods*, 2021, **13**, 3685–3692.
297 M. Yang, C. Wang, E. Liu, X. Hu, H. Hao and J. Fan, *Journal of Molecular Liquids*, 2021, **337**, 116438.
298 Y. Hu, Y. He, Z. Peng and Y. Li, *Biosensors and Bioelectronics*, 2020, **167**, 112490.
299 K. Dhara and R. M. Debiprosad, *Analytical Biochemistry*, 2019, **586**, 113415.
300 Y. Liu, P. Wu, X. Wu, C. Ma, S. Luo, M. Xu, W. Li and S. Liu, *Talanta*, 2020, **210**, 120649.
301 R. Zhu, W. Huang, X. Ma, Y. Zhang, C. Yue, W. Fang, Y. Hu, J. Wang, J. Dang, H. Zhao and Z. Li, *Analytica Chimica Acta*, 2019, **1089**, 131–143.
302 Y. Ji, X. Zou, W. Wang, T. Wang, S. Zhang and Z. Gong, *Microchemical Journal*, 2021, **167**, 106284.
303 Y. Han, Y. Bian and G. Wang, *Journal of Environmental Chemical Engineering*, 2023, **11**, 110750.
304 S. Wei, T. Li, X. Zhang, H. Zhang, C. Jiang and G. Sun, *Anal. Methods*, 2020, **12**, 5110–5119.
305 L. Liao, X. Lin, J. Zhang, Z. Hu and F. Wu, *Journal of Luminescence*, 2023, **264**, 120169.

View Article Online
DOI: 10.1039/D6TB00190D

View Article Online
DOI: 10.1039/D6TB00190D

Data Availability Statement

Data sharing is not applicable to this article as no new data were created or analysed in this review.